Thermal and Thermoelectric Properties of Molecular Junctions

Kun Wang, Edgar Meyhofer,* and Pramod Reddy*

Molecular junctions (MJs) represent an ideal platform for studying charge and energy transport at the atomic and molecular scale and are of fundamental interest for the development of molecular-scale electronics. While tremendous efforts have been devoted to probing charge transport in MJs during the past two decades, only recently advances in experimental techniques and computational tools have made it possible to precisely characterize how heat is transported, dissipated, and converted in MJs. This progress is central to the design of thermally robust molecular circuits and high-efficiency energy conversion devices. In addition, thermal and thermoelectric studies on MJs offer unique opportunities to test the validity of classical physical laws at the nanoscale. A brief survey of recent progress and emerging experimental approaches in probing thermal and thermoelectric transport in MJs is provided, including thermal conduction, heat dissipation, and thermoelectric effects, from both a theoretical and experimental perspective. Future directions and outstanding challenges in the field are also discussed.

1. Introduction

The idea of using individual molecules or nanoscale assemblies of molecules as functional electronic components or interconnects, also termed as "molecular electronics" (ME), holds significant promise to meet the increasing demand for miniaturization of electrical circuitry. The small size of molecules provides a unique opportunity to create electronic devices at a length scale of 1–3 nm which surpasses the dimensional limitations of conventional silicon-based technologies.[1] Moreover, the remarkable ability of molecules to self-assemble and the enormous diversity in molecular structures may also lead to fundamental discoveries of physical phenomena and functionalities that are not accessible with traditional semiconductor materials.[1a,2] Over the past two decades, ME has therefore spurred extensive experimental and theoretical efforts. Specifically, molecular junctions (MJs), created by trapping single molecules between two metallic electrodes, have proven be an

exceptional platform to probe quantum transport at the atomic and molecular level.[1c,3] Studies on MJs have contributed significantly to our understanding of the fundamental transport mechanisms in such systems and demonstrated a variety of intriguing charge transport phenomena, including conductance switching,[4] rectification,[5] gating (transistor effects),[6] negative differential resistance,[7] optoelectronic phenomena,[8] spintronic effects,[9] piezoelectricity[10] and quantum interference (QI) effects.[11]

Beyond the original vision of MJs as electronic components, it has also been predicted that MJs can act as efficient thermal and thermoelectric elements.[12] Further, recent advancements in the development of experimental techniques and computational tools have made it possible to probe how heat is carried, dissipated, stored, and converted in nanoscale systems.[13] Over the past decade, there has been growing interest in exploring thermal transport and thermoelectric energy conversion properties in MJs. Analogous to thermoelectric phenomena that arise in bulk materials a voltage differential also develops across an MJ when the electrodes of the MJ are held at different temperatures. In addition, charge carriers that transport energy across the junction also induce local heating or cooling at specific locations in the junction. Probing thermal transport and energy conversion in MJs is of paramount importance for addressing questions related to transport at the atomic and molecular level. For example, promising properties such as ultrahigh thermal conductivities and highly efficient thermoelectric energy conversion are expected to occur in carefully designed MJ systems, according to many theoretical proposals.[14] Thermal and thermoelectric studies on MJs may also shed light on nanoscale thermal management applications, such as local refrigeration,[15] thermal rectifier and transistors,[16] and thermal logic gates and memory,[17] which adds to the significance of the topic.

In this review, we describe recent progress in probing the thermal and thermoelectric properties of MJs from both experimental and theoretical perspectives. We present emerging experimental approaches used to characterize thermal and thermoelectric transport in MJs and the key insights obtained from these experimental and theoretical studies. The rest of this article is organized as follows: In Section 2, we briefly introduce the theoretical background of quantum transport in MJs; in Section 3, we discuss recent works on heat conduction, heat dissipation, and local heating/cooling in MJs; subsequently in Section 4, we survey the theoretical and experimental advancements in studying thermoelectric effects in MJs. Finally, in

Dr. K. Wang, Prof. E. Meyhofer, Prof. P. Reddy
Department of Mechanical Engineering
University of Michigan
Ann Arbor, MI 48109, USA
E-mail: meyhofer@umich.edu; pramodr@umich.edu
Prof. P. Reddy
Department of Materials Science and Engineering
University of Michigan
Ann Arbor, MI 48109, USA

The ORCID identification number(s) for the author(s) of this article can be found under https://doi.org/10.1002/adfm.201904534.

Section 5, we conclude by discussing current challenges and future perspectives of the field.

2. Basics of Quantum Transport in Molecular Junctions

2.1. Molecular Orbitals

Unlike the continuous and condensed energy-band dispersion of bulk materials, the energy levels of a molecule, the molecular orbitals, are discrete in energy and quantized (**Figure 1**). Electrons fill these orbitals, starting from the lowest available energy to the highest occupied molecular orbital (HOMO). In MJs the HOMO corresponds to the upper edge of the valence band of an inorganic semiconductor. The same equivalence exists between the lowest unoccupied molecular orbital (LUMO) in MJs and the lower edge of the conduction band in semiconductors. HOMO and LUMO are also referred to as the frontier molecular orbitals (FMO), i.e., they are orbitals that dominate charge transport. Electron transport in MJs through a specific molecule can be mediated either via the HOMO or LUMO, depending on which orbital is closer to the Fermi energy of the electrode. When a molecule bridges two bulk electrodes forming an MJ the discrete states merge into continuous states due to interactions with electrode states, which leads to intriguing transport properties in MJs.

2.2. Landauer Formalism of Quantum Transport

Charge transport through a short molecule is often described within the Landauer formalism,[18] also termed as Landauer–Büttiker formalism. Here, we briefly introduce how Landauer formalism can be applied to understand charge transport, thermal transport and thermoelectric transport problems in MJs. For detailed information of the Landauer approach, we refer readers to recent reviews.[19]

2.2.1. Electrical Conductance

In the Landauer formalism, electron transport through MJ is treated as a scattering problem. The energy distribution of electrons entering the MJ from the left (right) reservoir is governed by $f_{L(R)}$, where $f_{L(R)}$ is the Fermi–Dirac distribution associated with the left (right) electrode. The current passing from the left electrode across the molecule to the right electrode is given by[19a]

$$I = \left(\frac{2e}{h}\right) \int_{-\infty}^{\infty} \tau_e(E)(f_L - f_R)\, dE \tag{1}$$

where e is the charge of one electron, h is Planck's constant, E is energy, $\tau_e(E)$ is the transmission function for electrons passing from one electrode to the other electrode via the molecule. To obtain the electrical conductance of an MJ under a certain external bias V, one needs to average $\tau_e(E)$ over an energy window of width eV that is centered around the Fermi energy of the electrode. In the small voltage, low-temperature limit,

Kun Wang received a B.S. in physics from Shandong University, China in 2011 and a Ph.D. in physics from the University of Georgia, USA in 2016. He is currently a postdoctoral research fellow in the Department of Mechanical Engineering at the University of Michigan, Ann Arbor. His research interests include quantum transport, energy conversion, plasmonics and sensing in nano/molecular-scale devices.

Edgar Meyhofer received a B.S. in biology from the Universität Hannover in Germany, and a M.S. from Northeastern University in Boston. In 1991 he earned a Ph.D. from the University of Washington, Seattle. Since 2001 he has been a Professor of Mechanical Engineering and Biomedical Engineering at the University of Michigan in Ann Arbor. His current interests include nanoscale radiative heat transfer, energy transport in molecular junctions and nanoscale energy conversion.

Pramod Reddy received a B.Tech. and M.Tech. in mechanical engineering from the Indian Institute of Technology, Bombay in 2002 and a Ph.D. in applied science and technology from the University of California, Berkeley in 2007. He is currently a professor in the departments of Mechanical Engineering and Materials Science and Engineering at the University of Michigan, Ann Arbor.

Equation (1) can be simplified and the electrical conductance G_e of the MJ can be expressed as[19b]

$$G_e = \frac{I}{V} = G_0\, \tau_e(E_F) \tag{2}$$

where G_0 is the quantum of electrical conductance and has a value of $\frac{2e^2}{h} \approx 77.48\,\mu S$ and E_F is the Fermi energy (chemical potential) of the electrode materials. Note that the transmission
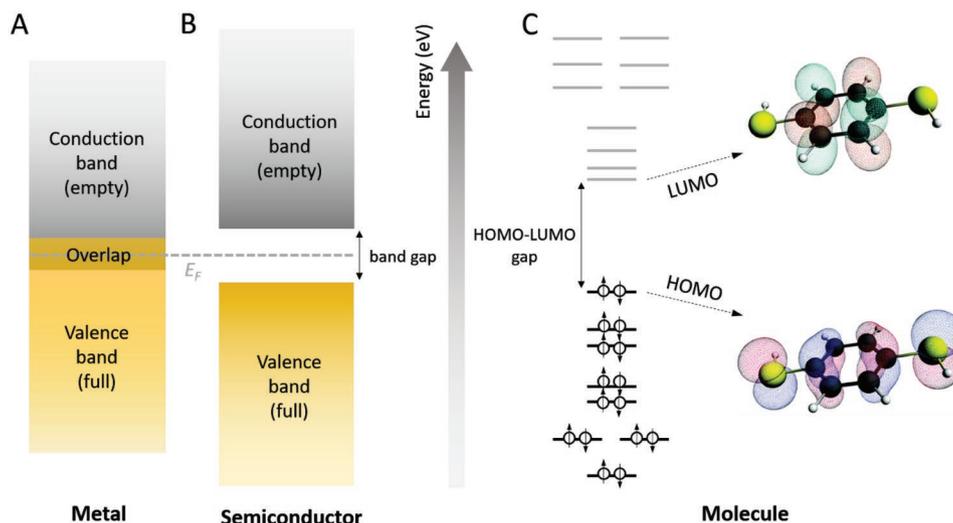
Figure 1. Energy band diagram of A) metal, B) semiconductor, and C) molecular orbitals. The isosurface of HOMO and LUMO of 1,4-benzenedithiol molecule is shown on the right panel in (C). C) Reproduced with permission.[1e] Copyright 2015, Royal Society of Chemistry.

function of an MJ depends on the electronic structure of the molecule and the coupling at the molecule–electrode interfaces, therefore it varies from one MJ to another depending on the exact composition and geometry of the junction.

The above expressions (Equations (1) and (2)) assume that an electron remains phase coherent as it passes from one electrode to the another and does not undergo inelastic scattering.[19b] However, as the length of a molecule increases, the probability of inelastic scattering (e.g., from phonons or other electrons) becomes non-negligible and the above expressions may require further correction or modification.

2.2.2. Thermal Conductance

When a temperature difference ΔT is present between the two electrodes of an MJ, heat flows from the hot side to the cold side across the molecule (**Figure 2**c). Similar to bulk materials, there are two basic contributions to the thermal conduction of MJs, electrons, and phonons. Therefore, the thermal conductance κ of an MJ is usually considered to be the sum of thermal conductance of electrons κ_e and thermal conductance of phonons κ_{ph}: $\kappa = \kappa_e + \kappa_{ph}$. Given that the inelastic mean free path for electrons (tens of nanometers) and phonons (a few nanometer to tens of nanometers) in the electrodes is larger than the typical dimension of a short molecule (usually less than three nanometers), transport in MJs can be modeled within the Landauer approach, where one assumes that the transport, both electronic and phononic, is dominated by elastic scattering.[20] The heat currents in MJs have contributions from both electrons J_e and phonons J_{ph} and can be estimated from[18a,21]

$$J_e = \frac{2}{h} \int_{-\infty}^{\infty} (E - E_F) \tau_e(E)(f_L - f_R) \, dE \qquad (3)$$

and

$$J_{ph} = \int_0^{\infty} (h\nu) \tau_{ph}(\nu)(g_L - g_R) \, d\nu \qquad (4)$$

where ν is the phonon frequency and $\tau_{ph}(\nu)$ is the transmission function for phonons and g_L and g_R denote the Bose–Einstein distributions for the left and the right thermal reservoirs, respectively, and depend on the temperature of the electrodes.

Recent theoretical studies suggest that a more rigorous calculation of thermal conductance of MJs should also consider the contribution of photons because thermal radiation or photon tunneling may occur in the nanoscale gap between the two electrode surfaces of an MJ.[22] We note that there are several approaches to calculate the thermal conductance of an MJ, such as density functional theory (DFT)-based methods, molecular dynamic simulations, and tight binding models, which will not be discussed here.[13b]

2.2.3. Thermopower (Seebeck Coefficient) S and the Figure of Merit ZT of MJs

Similar to bulk thermoelectric materials, when a temperature difference ΔT is present at the two terminals of an MJ, an open-circuit voltage ΔV is created due to the Seebeck effect, and its value (for small temperature differentials, i.e., when the temperature differential is much smaller than the ambient temperature, i.e., ≈10 K at room temperature) is proportional to the magnitude of the temperature difference (Figure 2b). The relation between ΔV and ΔT is given by: $\Delta V = -S\Delta T$, where S is the thermopower or Seebeck coefficient of the MJ.[13c] Within the Landauer framework, under the assumption that the transmission function of the MJ is smooth and has no significant change within an energy range of $k_B T$ around the electrode's Fermi energy E_F, the thermopower S of an MJ is given by[12,23]

$$S = -\frac{\pi^2 k_B^2 T}{3|e|} \frac{\partial \ln(\tau(E_F))}{\partial E_F} \qquad (5)$$

From Equation (5), we see that the sign of Seebeck coefficient can be positive or negative, depending on the sign of the slope of the transmission function at the Fermi energy E_F.
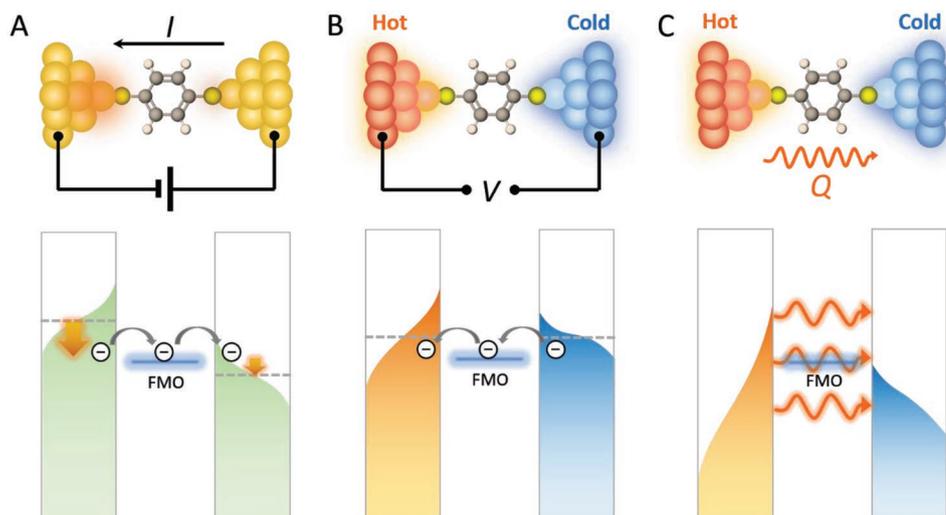
Figure 2. Molecular junction schematics (upper panels) and the corresponding energy profiles (lower panels) for three scenarios: A) heat dissipation in current carrying molecular junctions with no temperature gradient across the junction. Orange arrows in bottom panel indicate heat dissipation. When current flows across the junction, two situations may occur: 1) Peltier cooling on one electrode and Joule heating on the other electrode and 2) Joule heating on both electrodes. Under small external biases, when $|V| < 2|ST|$ (V is the applied bias, S is the Seebeck coefficient of the junction, and T is the ambient temperature), cooling is expected to occur on one of the electrodes when SV, the product of Seebeck coefficient and the applied bias, is negative. For the rest situations, Joule heating occurs on both electrodes. B) Thermoelectric transport across the junction under an applied temperature difference ($T_{hot} - T_{cold}$). Under open-circuit setup (no external applied bias), the thermovoltage generated due to temperature difference across the molecular junction, i.e., Seebeck effect, drives current flow through the junction. C) Thermal transport (contributed from both phonons and electrons) when a temperature difference is applied across the junction. Thermal transport through molecular junction is predominantly facilitated by heat conductions via phonons. The heat conduction via electrons is usually very small. Note that the frontier molecular orbital (FMO) is shown in the energy profile of each scenario.

The sign of the Seebeck coefficient is related to the nature of charge carriers: The Seebeck coefficient is positive for hole-dominated transport and negative for electron-dominated transport. Therefore, measurements of Seebeck coefficient of MJs are of great importance in determining the dominant transport mechanism and the location of frontier molecular orbitals in MJs.

To evaluate the applicability of a thermoelectric material for energy conversion, one must consider the efficiency of the material for converting thermal to electrical energy or for refrigeration. This efficiency is a monotonically increasing function of the dimensionless figure of merit, ZT. Similar to the case of a bulk material, the figure of merit (ZT) of an MJ is also given by[13c]

$$ZT = \frac{G_e S^2 T}{\kappa} \tag{6}$$

where G_e, S, and κ are the electrical conductance, Seebeck coefficient, and thermal conductance of the MJ, respectively. Considering the Wiedemann–Franz law, which defines the ratio of thermal conductance due to electrons to the electrical conductance is proportional to temperature $L_0 T = \kappa_e / G_e$, where L_0 is the Lorenz number, one can rewrite Equation (6) as

$$ZT = \frac{G_e S^2 T}{\kappa_e + \kappa_{ph}} = \frac{G_e S^2 T}{\kappa_e \left(1 + \frac{\kappa_{ph}}{\kappa_e}\right)} = \frac{S^2}{L_0 \left(1 + \frac{\kappa_{ph}}{\kappa_e}\right)} \tag{7}$$

From Equation (7), it is clear that ZT of an MJ is dominated by the competition between Seebeck coefficient and the ratio of phononic thermal conductance to electronic thermal conductance. To increase the figure of merit, one needs to either increase the Seebeck coefficient or suppress the relative contribution of phononic thermal conductance with respect to electronic thermal conductance. We therefore suggest the ratio of κ_{ph}/κ_e as a function of temperature deserves to be explicitly illustrated in future theoretical studies.

2.2.4. Heat Dissipation

It is well known that current flow is often accompanied by heat dissipation (Joule heating), and in bulk materials the magnitude of the power dissipation is related to current density and electrical resistivity of the material. As charge transport through a nanoscopic molecule is largely elastic, heat dissipation in MJs is fundamentally different. In fact, for the case of a short molecule, heat dissipation due to inelastic scattering (i.e., electron–electron and electron–phonon interactions) only occurs in the two electrodes (Figure 2a).[24] Using the Landauer theory, heat dissipation in the left and right electrodes of an MJ, Q_L and Q_R, can be described respectively as[25]

$$Q_L = \frac{2}{h} \int_{-\infty}^{\infty} (E_{FL} - E)\, \tau_e(E)(f_L - f_R)\, dE \tag{8}$$

and

$$Q_R = \frac{2}{h} \int_{-\infty}^{\infty} (E - E_{FR})\, \tau_e(E)(f_L - f_R)\, dE \tag{9}$$

where E_{FL} and E_{FR} are the Fermi energies (chemical potential) of the left and right electrode.

3. Thermal Properties of Molecular Junctions

In this section, we give an overview of recent theoretical and experimental efforts on probing thermal transport in MJ systems featuring both single molecules and self-assembled monolayers (SAMs). Research topics of interest include study of thermal conductance, heat dissipation, and local heating or cooling in MJs. For each topic, we begin by first describing the computational and theoretical works and then discuss the adopted experimental techniques and important experimental discoveries in the field.

3.1. Thermal Conduction in MJ

3.1.1. Theoretical Studies

The quantitative description of heat flow in bulk materials was originally described by Fourier's law which states that the thermal current density ($\vec{J}_{th}$) induced by a temperature gradient $\vec{\nabla}T$ is given by $\vec{J}_{th} = -\kappa\vec{\nabla}T$, where κ is the thermal conductivity.[13b] Testing the validity of this description in a nanoscale system such as atomic and molecular chains has been of major interest for many decades. Specifically, early computational works using nonequilibrium molecular dynamics (NEMD) and equilibrium Green–Kubo methods explored heat transport in 1D lattice chains of monoatomic particles interacting with each other via

harmonic potentials.[26] They found that a divergence in thermal conductivity is to be expected for various interatomic configurations, which is in clear disagreement with Fourier's law. These works also suggest that such divergences may be a general feature of 1D chains and the classical Fourier's law may not be applicable for thermal transport in 1D systems.

Compared to early computational studies of thermal transport in 1D lattice chains, which did not consider the effects of electrodes, MJs represent a more experimentally tractable platform which also captures the coupling between the 1D molecular chain and the electrodes. Heat conduction in MJs was first theoretically studied in alkane molecules, a relatively simple molecular system consisting of a chain of carbon atoms that is covalently bonded to metal electrodes at both ends. For example, using a Landauer-type expression for phononic heat transport (a generalized Langevin equation), Segal et al. studied the dependence of the thermal conductance of alkanes as a function of molecular length and temperature.[27] They reported that the thermal conductance of alkanes has an interesting dependence on the number (N) of carbon atoms: for $N = 2$–4, the conductance rises with chain length and with increasing length declines monotonically from $N = 5$ to about $N = 15$ atoms. When the number of atoms increases to be greater than 15 then the conductance is predicted to be length independent (**Figure 3**a). It was suggested that such dependence of heat conduction results from a balance of three factors: i) the molecular frequency spectrum with respect to the cutoff
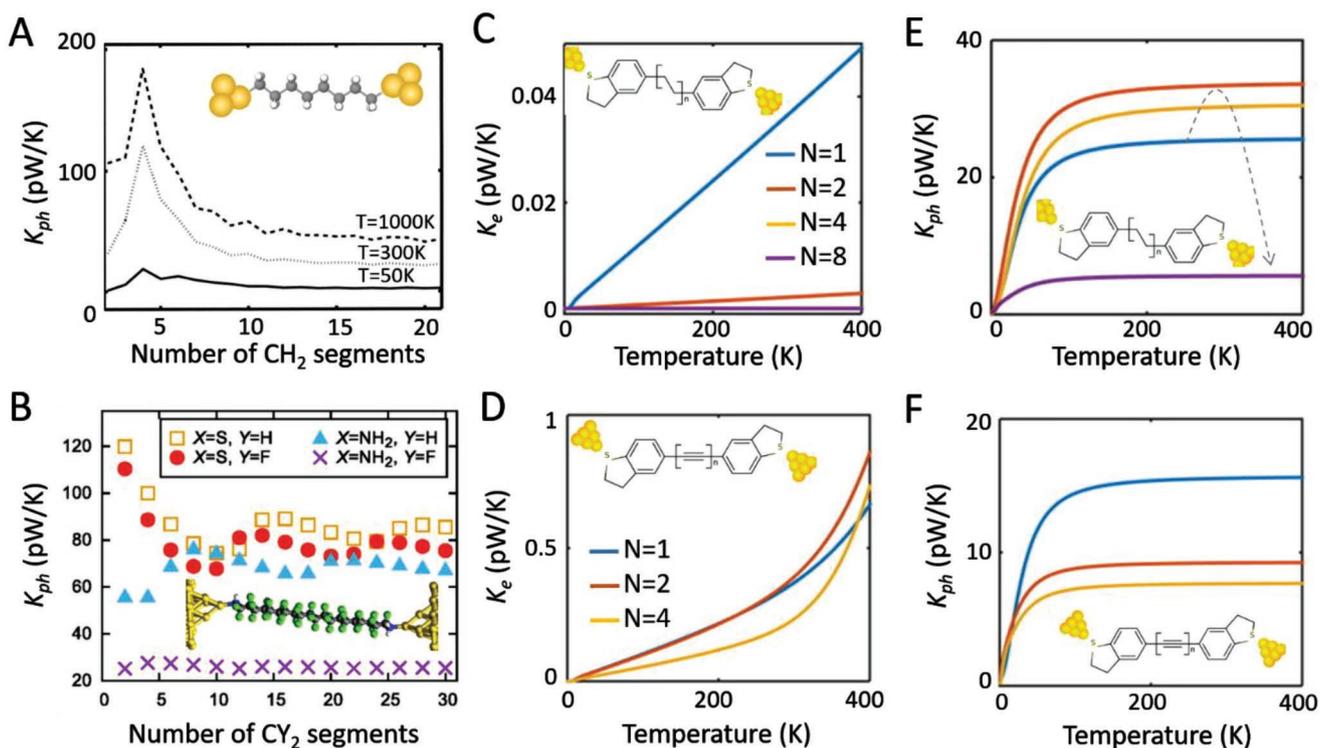

Figure 3. Calculated thermal conductance of single molecule junctions. A) Thermal conductance of alkane molecules as a function of chain length at different temperatures. Reproduced with permission.[27] Copyright 2003, American Institute of Physics (AIP) Publishing. B) Room temperature ($T = 300$ K) phonon thermal conductance as a function of the number of CY$_2$ units (Y = H, F) in the molecule for both anchoring groups, thiol (S) and amine (NH$_2$). Reproduced with permission.[29] Copyright 2016, American Physical Society. (C) and (D) show the electronic thermal conductance versus temperature of alkanes and oligoynes in different lengths, respectively. (E) and (F) show the phononic thermal conductance versus temperature of alkane and oligoynes, respectively. C–F) Reproduced with permission.[28] Copyright 2015, American Chemical Society.

**ADVANCED
SCIENCE NEWS**
www.advancedsciencenews.com

**ADVANCED
FUNCTIONAL
MATERIALS**
www.afm-journal.de

frequency of the thermal reservoirs, ii) the degree of localization of the molecular normal modes, and iii) the molecule-heat reservoirs coupling. The fact that molecular modes at different frequency regimes have difference localization properties essentially gives rise to an intricate dependence of the heat conduction on molecular length at different temperature.

Recently, Sadeghi et al.[28] used DFT-based methods to calculate both the electronic and phononic thermal conductance of alkane chains ($N = 1, 2, 4, 8$) and oligoynes ($N = 1, 2, 4$), respectively. As illustrated in Figure 3c–f, for alkane junctions, they identified a similar dependence of phononic thermal conductance on molecular length, an initial increase in the thermal conductance molecules upon increasing chain length, and a subsequent decrease as the molecular length increases further (Figure 3e). However, they also found that due to the more rigid nature of oligoynes, the phononic thermal conductances of oligoynes are counterintuitively lower than those of the corresponding alkanes and decrease monotonically with increasing length (Figure 3f). More importantly, it was found that for both molecular species, the thermal conductance contribution from phonons is much larger than that from electrons ($\approx$700 times larger for alkane junctions and $\approx$30 times larger for oligoynes cases), suggesting a phonon dominant thermal transport mechanism in these MJs. More recently, Klöckner et al. used an ab initio approach combining DFT and a nonequilibrium greens function method to study the thermal

conductance of alkanes and polytetrafluoroethylene (PTFE) molecules (where H atoms in alkanes are replaced by F atoms) connected to Au electrodes via thiol (−SH) or amine (−NH$_2$) linker groups (Figure 3b).[29] They found that i) the room-temperature phononic thermal conductances is fairly length independent for chains with more than five methylene units and ii) the thiol-terminated MJs yield higher thermal conductance than the amine-terminated ones, indicating that the efficiency of the thermal transport is strongly influenced by the strength of the metal–molecule coupling. The dependence of thermal conductance on molecular length for alkane chains reported by Klockner et al. is somewhat different from the findings by Segal et al.[27] as can be seen from a comparison of Figure 3a,b. The reason for this discrepancy is unclear. Nevertheless, these findings clearly imply that the thermal conduction in molecular junctions is mainly dominated by contributions from phonons and it depends on both the molecular structure and the molecule–electrode contacts.

Thermal transport in more complex molecules, such as π-conjugated molecules, has also been computationally explored. For example, Markussen studied the phononic thermal conductance of both linear- and crossconjugated oligo(phenylene ethynylene) (OPE) MJs.[30] Their computational results, as illustrated in **Figure 4**a, reveal that the phonon transmission function in crossconjugated molecules, such as meta-connected benzene, exhibits destructive quantum interference
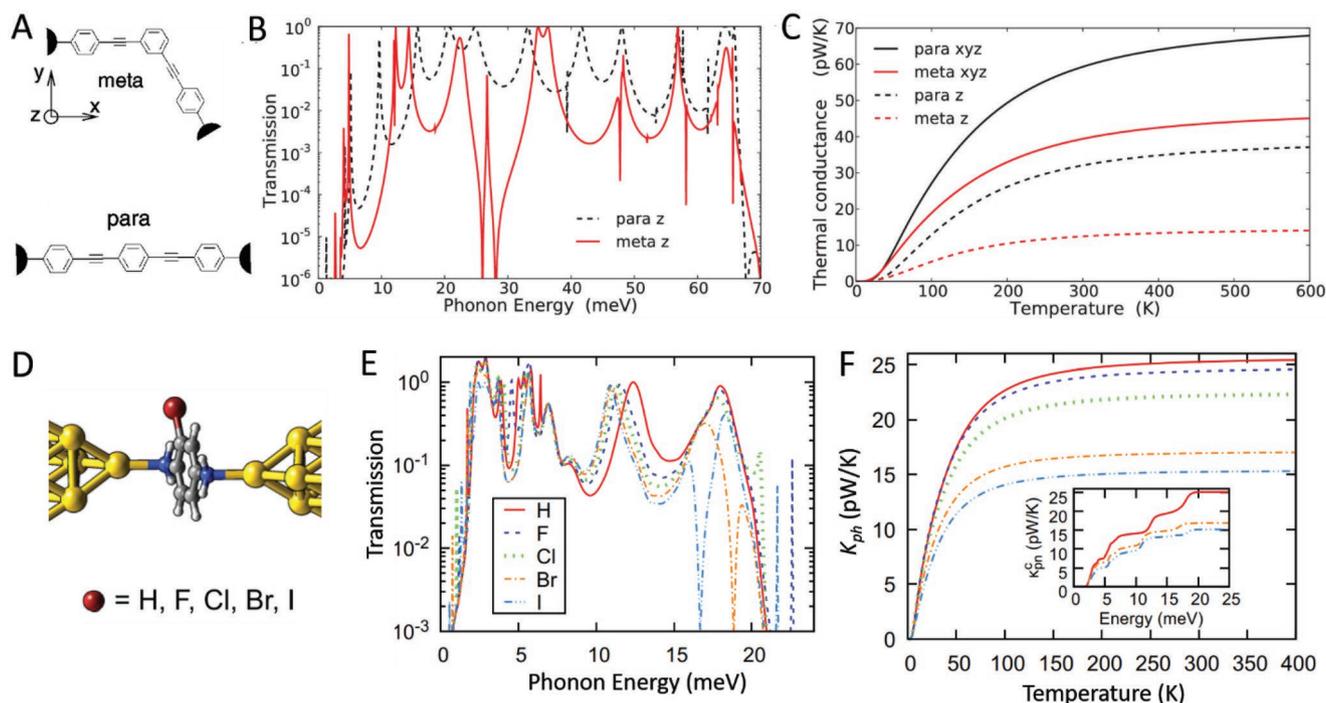

Figure 4. Calculated thermal conductance of π-conjugated molecular junctions and the influence of quantum interference. A) Structure of meta- and para-OPE3. B) Phonon transmission functions for meta- (solid red) and para-OPE3 (dashed black) calculated from only out-of-plane (z-direction) motion. C) Thermal conductance versus temperature for meta (red) and para-OPE3 in the two cases of only out-of-plane motion (dashed lines) and inclusion of motion in all (x, y, z)-directions (solid lines). A–C) Reproduced with permission.[30] Copyright 2013, AIP Publishing. D) Schematics of Au–benzenediamine–Au junction, with one H atom of the benzene molecule substituted by a halogen atom (X = F, Cl, Br, I). E) Phonon transmission as a function of energy for junctions with different substituents. F) The corresponding phononic thermal conductance as a function of temperature for the different benzenediamine derivatives. The inset shows the room-temperature cumulative thermal conductance as a function of energy for the junctions with X = H, Br, I. D–F) Reproduced with permission.[32] Copyright 2017, American Physical Society.

features similar to those observed for electron transport in the linear and crossconnected OPE molecules.[31] More importantly, the destructive interference features of those crossconjugated molecules significantly reduce the thermal conductance with respect to linear conjugated analogues. Recently, Klockner et al. used a DFT-based first-principles method to analyze the coherent phonon transport in single-molecule junctions made of several benzene derivatives (Figure 4d).[32] They showed that the thermal conductance of these MJs can be tuned via the inclusion of substituents, which also induces destructive interference effects and results in a decrease of the thermal conductance with respect to the unmodified molecules (Figure 4f). These interference effects manifest themselves as antiresonances in the phonon transmission (Figure 4e), whose energy positions can be tuned by varying the mass of the substituents.

In addition to single molecule studies, heat conduction through SAM of molecules has also received considerable attention due to growing interest in thin film electronics and interface sciences. A summary of representative computational results of the thermal conductance of various MJs based on SAMs is shown in **Figure 5**. It has been shown by several groups that the thermal conductance of SAM-based MJs is

nearly independent of molecular length and temperature.[33] For example, Luo et al.[33a] performed NEMD calculations on Au–SAM–Au junctions and found the thermal conductance to be insensitive to molecular length and temperature (Figure 5a). Duda et al.[33c] later observed similar phenomena when calculating the interfacial thermal conductance (ITC) of Au–SAM junctions (Figure 5b). In contrast, Hu et al.[34] used molecular dynamics simulations to calculate the thermal conductance of Au–SAM–Si junctions (one Au electrode replaced by Si) and observed distinct oscillations in the phonon transmission function with a strong dependence on the phonon frequency. Such behavior is a key signature of a phonon interference effect. Further, they found that this interference effect diminishes as molecular length (SAM thickness) is increased.

Recently, solid–SAM–liquid junctions have gained considerable attention as they are critical for a wide range of applications such as solar thermal evaporation and nanofluids. Goicochea et al.[35] studied the thermal conductance of silica–SAM–water junctions (Figure 5c). They found that when the silica surface is coated with a monolayer of alkysilanol ($-Si(OH)_2-(CH_2)_n$ $-OH$), the thermal conductance of silica–SAM–water junction is three times higher than that of bare silica–water junctions,
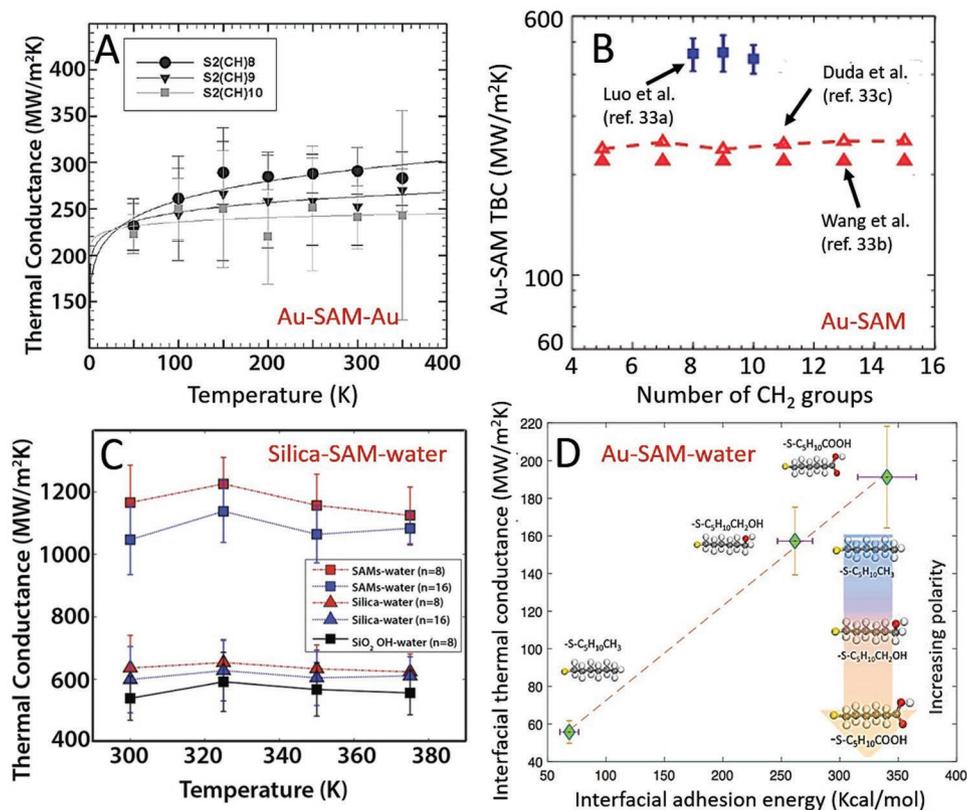

Figure 5. Calculated thermal conductance of self-assembled monolayer (SAM) junctions. A) Thermal conductance of Au–alkanethiol–Au junctions in different lengths as a function of temperature. Reproduced with permission.[33a] Copyright 2010, American Society of Mechanical Engineer. B) Thermal conductance across Au–alkanethiol monolayer interface as a function of molecular length calculated by different groups. Reproduced with permission.[33a] Copyright 2009, American Society of Mechanical Engineers; Reproduced with permission.[33b] Copyright 2007, American Association for the Advancement of Science; Reproduced with permission.[33c] Copyright 2011, AIP Publishing. C) Thermal conductance of SiO₂–SAM–water junctions as a function of temperature. The SAM are formed by alkysilanol ($-Si(OH)_2-(CH_2)_n-OH$). Reproduced with permission.[35] Copyright 2011, American Society of Mechanical Engineer. D) Interfacial thermal conductance (ITC) as a function of the interfacial adhesion energy for water contacting Au surfaces functionalized with different molecules. Stronger interfacial adhesion energy leads to larger ITC. The dashed line is a linear fit. Reproduced with permission.[36] Copyright 2018, American Chemical Society.
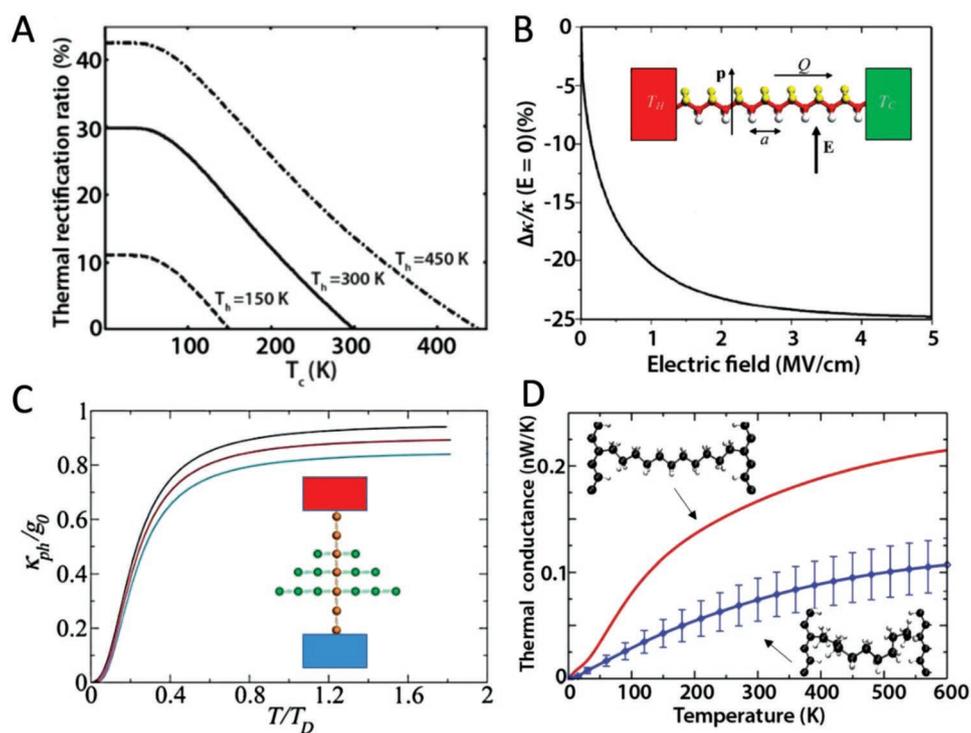
Figure 6. Theoretical proposals for tuning thermal transport in molecular junctions. A) Thermal rectification ratio in a two-level phonon model as a function of the cold reservoir temperature T_c when the hot reservoir temperature T_h is constant. Reproduced with permission.[16b] Copyright 2005, American Physical Society. B) Thermal conductance as a function of externally applied electric field. The electric field modulates the dipole moments of the monomers. Reproduced with permission.[37] Copyright 2010, American Physical Society. C) Thermal conductance of a Christmas tree-like molecular junction as a function of temperature. Phonon transport along the trunk is suppressed by Fano resonances associated with internal vibrational modes of the branches and that thermal conductance is suppressed most effectively in molecules with pendant branches of different lengths. Reproduced with permission.[41] Copyright 2017, Wiley-VCH. D) Thermal transport through an alkane chain bridged between graphene electrodes under mechanical compression (blue) and extension (red). The thermal conductance of the compressed junction drops by half in comparison to the extended junction. Reproduced with permission.[38] Copyright 2015, American Chemical Society.

suggesting a strategy to improve thermal conductance at the solid–liquid interfaces. This observation is attributed to the fact that the silica surface becomes hydrophilic after SAM modification on the solid surface. To tune thermal transport across solid–water interfaces, Huang et al.[36] reported that the electrostatic interactions between the polar functional group of SAMs attached on solid surface can attract water molecules closer to the SAM surface, which increases the power exchanged between solid and water atoms and leads to an enhancement in the interfacial thermal conductance (Figure 5d).

The ability to control thermal transport in MJs, including contributions from both electrons and phonons, is of paramount importance for applications in regulating heat flow at the nanoscale and for the development of highly efficient thermoelectric devices. Inspired by unusual transport features seen in theoretical simulations, several strategies have been proposed (**Figure 6**). For example, it has been suggested that MJs can function as thermal rectifiers[16a,b] (unidirectional heat flow across MJs), field-effect thermal transistors[37] (by reversibly alternating between acoustic and optical modes), thermal modulators[38] (by mechanically modulating the junction separation), heat pumps,[39] and heat rachets[40] (directed heat flow even when the net average temperature difference across the junction is zero).

Given that thermal transport across MJs is usually dominated by phonons, minimizing the phononic thermal conductance of MJs is highly desirable, especially for the design of high efficiency thermoelectric devices. This has led to several theoretical proposals. Harnessing the phonon quantum interference effect has been proposed as one promising approach to suppress phononic thermal transport in MJs.[30,32] Recently, Famili et al.[41] proposed "Christmas tree"-like molecules composed of "a long trunk," along which phonons can propagate, attached to pendant molecular branches (Figure 6c). Their calculations suggested that phonon transport along the trunk is suppressed by Fano resonances associated with internal vibrational modes of the branches and that thermal conductance is suppressed most effectively in molecules with pendant branches of different lengths. Li et al.[38] studied thermal transport through an alkane chain bridged between graphene electrodes under mechanical compression and extension (Figure 6d). They found that the thermal conductance of the compressed junction drops by half in comparison to the extended junction, suggesting a mechanical approach to suppress the thermal conductance. Other strategies include tailoring π-stacked molecules with each stacking layer weakly coupled to each other and tuning the mismatch in phonon density of states between the molecule and electrode.[28,42]

**ADVANCED
SCIENCE NEWS**
www.advancedsciencenews.com

**ADVANCED
FUNCTIONAL
MATERIALS**
www.afm-journal.de

3.1.2. Experimental Studies

Conceptually, measurement of the thermal conductance of MJs is straightforward; however, first experimental results have only been obtained very recently. This is mainly because the heat current of MJs is usually very small and can be easily masked in the thermal noise from the background. The technical limitation in quantifying small heat current had remained a major hurdle until recent progress in high resolution microcalorimetry techniques.[24,33b,43]

Due to the comparatively large heat current in SAMs (in comparison to MJs), which allow heat flow through many molecules simultaneously, experimental measurements of the thermal conductance were first performed in an SAM-based MJ system[44] as opposed to single molecule MJs. For example, Wang et al.[45] measured the thermal conductance of Au–alkanedithiol–GaAs junctions. The molecular junction was created using a nanotransfer printing technique, where a thin Au film, patterned on a silicon stamp, was transferred onto a GaAs substrate that was chemically functionalized with an SAM of target molecules. The patterned Au film was employed as a heater/thermometer to measure thermal conductivity of an SAM using the 3ω method.[46] As shown in **Figure 7**a, the measured thermal conductance of alkane SAM was insensitive

to molecular length (monolayer thickness). In another study, Wang et al.[33b] probed heat transport through SAMs of long-chain alkanedithiol molecules anchored to a gold substrate by ultrafast heating of the gold with femtosecond laser pulses (Figure 7b). In their study, a nonlinear coherent vibrational spectroscopy technique was employed to detect the ultrafast, thermally induced disorder when heat reached the methyl groups at the chain ends. They found that the leading edge of the heat burst traveled ballistically along the chains at a velocity of ≈1000 m s^{-1} and estimated the molecular thermal conductance per chain to be ≈50 pW K^{-1}. However, the flow of heat into the chains was found to be limited by the interfacial conductance. These initial thermal transport measurements on solid–SAM–solid junctions not only shed light on the influence of molecular structure, chemical composition, and interface effects, they also led to the development of strategies to tune the thermal conductance of SAMs.[13b,38,41]

Several studies have also explored the impact of solid–molecule interface on the thermal conductance. For example, Losego et al.[47] studied thermal transport in Au–SAM–quartz junctions where termination chemistries of SAMs were varied systematically (Figure 7d). Using a combination of ultrafast pump–probe techniques (time-domain thermal reflectance, TDTR, and picosecond acoustics) and laser spallation experiments, they
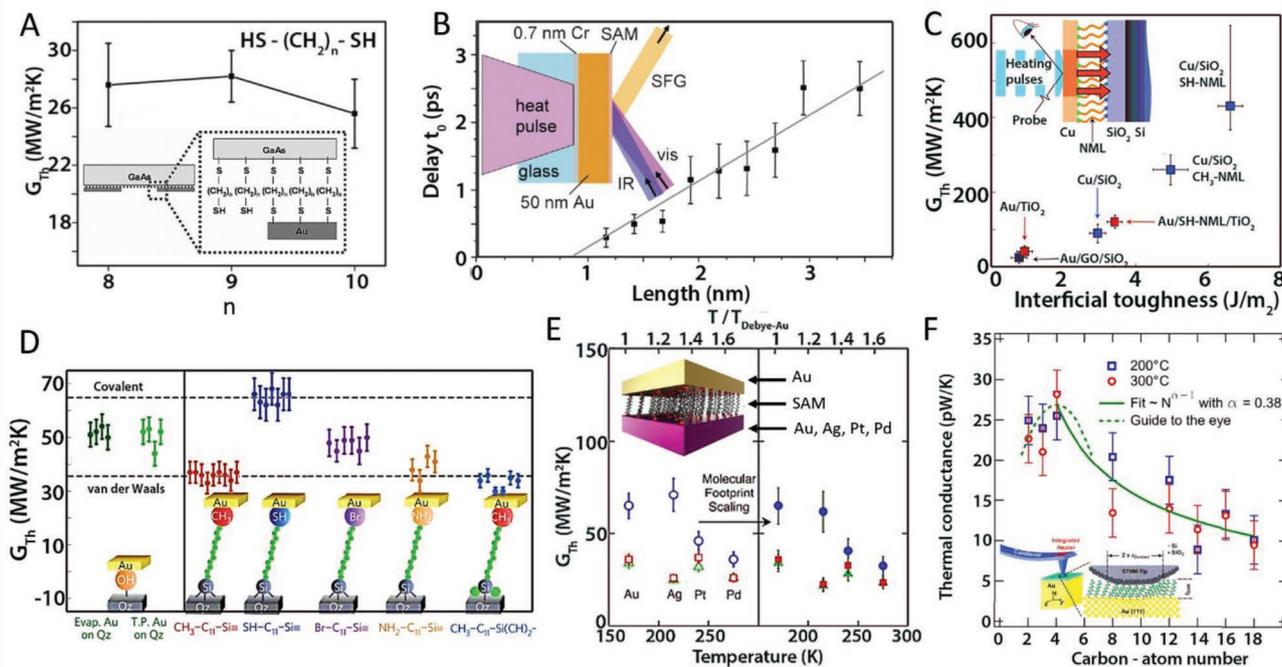

Figure 7. Measured thermal conductance of self-assembled monolayer junctions. A) Room temperature thermal conductance of Au–alkanedithiol–GaAs junctions as a function of molecular length. Inset: Sample schematic. Reproduced with permission.[45] Copyright 2006, American Physical Society. B) The delay time, that is, the time for the heat burst to travel across the Au–alkanethiol junction and arrive the methyl head group, as a function of molecular length. Inset: Schematic of the experimental setup. Reproduced with permission.[33b] Copyright 2007, American Association for the Advancement of Science. C) Thermal conductance of metal–SAM–dielectric junctions measured with TDTR technique. Inset: Schematic of time-domain thermal reflectance (TDTR) setup. Reproduced with permission.[48] Copyright 2012, Springer Nature. D) Thermal conductance of alkane based molecular junctions with different molecule–electrode interfaces (covalent bond or van der Waals interaction). Reproduced with permission.[47] Copyright 2012, Springer Nature. E) Impact of vibration mismatch on thermal conductance of SAM junctions. The vibrational mismatch is induced using metallic electrodes (Au, Ag, Pt, Pd) with different Debye temperatures (i.e., cutoff phonon frequencies). Reproduced with permission.[49] Copyright 2015, American Chemical Society. F) Thermal conductance of Au–alkanedithiol–SiO$_2$ junctions as a function of molecular length measured with scanning thermal probe technique. Reproduced with permission.[50] Copyright 2014, American Physical Society.

**ADVANCED
SCIENCE NEWS**
www.advancedsciencenews.com

**ADVANCED
FUNCTIONAL
MATERIALS**
www.afm-journal.de

demonstrated that junctions with covalent bonds at the interfaces exhibited higher thermal conductance than those based on van der Waal interactions at the interface. They also observed a linear dependence of interfacial thermal conductance on the density of covalent bonds, suggesting that phonon transport dominates across the interfaces. O'Brien et al.[48] measured the thermal conductance of metal–SAM–dielectric junctions, where the SAM was composed of organosilane molecules with different terminal groups (−SH and −CH₃) (Figure 7c). Two dielectric materials, SiO_2 and TiO_2, were studied. Compared with the thermal conductance of direct metal–dielectric contact, the thermal conductance across metal–dielectric interfaces can be enhanced by a factor of 4 after introducing the SAM. Based on their experimental results, they argued that this enhancement is because the SAM facilitates better phonon transport through both Au–SAM and SAM–dielectric interfaces. They also showed that junctions with -thiol (SH−) terminal groups have a higher thermal conductance over those with methyl (−CH₃) groups.

More recently, Majumdar et al.[49] studied the influence of vibrational mismatch of metal electrodes (Au, Ag, Pt, and Pd) on the thermal conductance of Au–alkanedithiol–metal junctions. By employing a frequency-domain thermal reflectance technique, they demonstrated that Au–alkanedithiol–Au junctions yield a two-times higher thermal conductance compared to that of Au–alkaneditiol–Pd junctions. This indicates that the vibrational modes of the electrodes play a significant role, even though the thermal carriers of the metal electrodes are electrons. In another set of studies, by taking advantage of scanning probe microscopy, a thermal conductance measurement technique based on scanning thermal probes (scanning probes capable of detecting heat fluxes) has also been developed. For instance, Meier et al.[50] probed the thermal conductance of Au–alkanedithiol–SiO_2 junctions by employing a scanning thermal probe as one electrode. They reported that the thermal

conductance of the junctions first increases with molecular length then decreases and eventually remains unchanged as molecular length reaches a critical length (Figure 7f). This report is consistent with previous theoretical predictions on single molecule junctions by Segal et al.[27]

While important first insights into the thermal properties of MJs were obtained by probing transport in SAMs, a number of experimental uncertainties and challenges in the interpretation of the data continue to press for the development of experimental tools to measure thermal transport through a single MJ. Unfortunately, progress toward reliable measurements has been lacking significantly behind, principally because the heat flux through a single molecule is very small and ultrahigh calorimetric resolution at the level of a few picowatts is required. Toward this goal, thermal sensing techniques based on scanning probe approaches have been developed very recently to probe thermal transport in metal atomic junctions.[43,51] For example, Cui et al.[43] developed custom-fabricated, calorimetric scanning probes with pW resolution to measure the thermal conductance of gold and platinum single atom junctions (**Figure 8**). They found that the thermal conductance of gold and platinum single-atom junctions is quantized at room temperature and showed that the Wiedemann–Franz law relating thermal and electrical conductance is satisfied even in single-atom contacts. Mosso et al.[51] also explored thermal transport in Au atomic junctions by employing a microfabricated device where the temperature sensing element was a suspended membrane with an integrated thermal sensor and reported the validity of the Wiedemann–Franz law. Given the high thermal resolution and excellent performance of these techniques in atomic junctions, they were expected to enable thermal transport studies in single molecule junctions.

Not surprisingly, the first measurements of thermal conductance measurement of single molecule junctions featuring
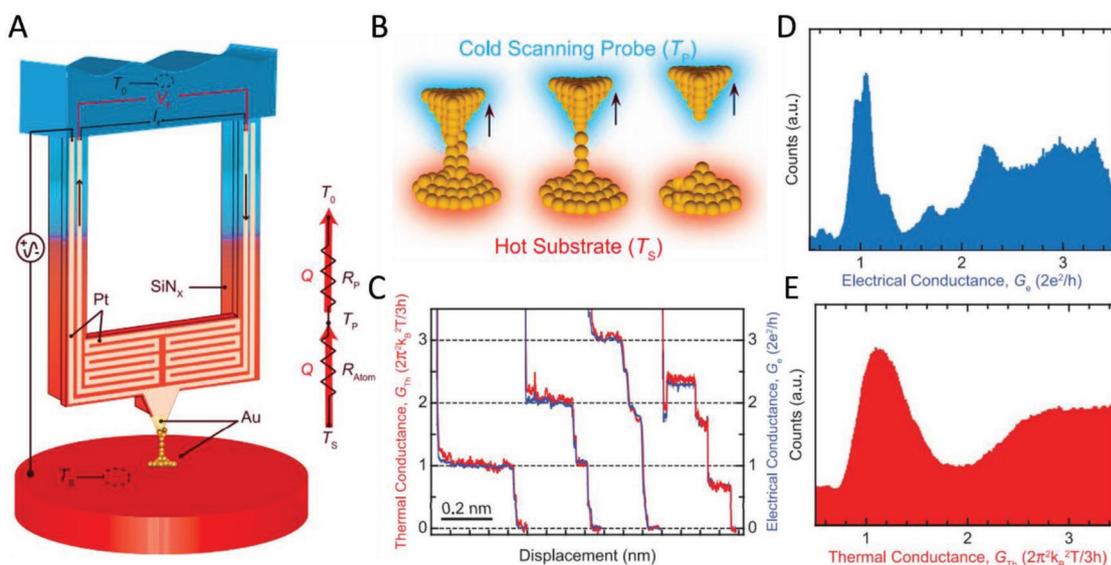

Figure 8. Quantized thermal conductance of single-atom junctions. A) Schematic of a calorimetric scanning thermal microscopy probe. B) Schematics of the formation-to-rupture evolution of Au atomic chains upon tip retraction. C) Simultaneously measured electrical (blue) and thermal (red) conductance traces of Au–Au atomic junctions. D,E) Electrical and thermal conductance histograms constructed from concurrently measured electrical and thermal conductance traces. Reproduced with permission.[43] Copyright 2017, American Association for the Advancement of Science.

Au–alkanedithiol–Au junctions were very recently reported by Cui et al.[52] using the calorimetric scanning thermal (C-SThM) probes which enabled the quantification of thermal conductance of single atomic junctions in their early work. They demonstrated that when used in conjunction with a time-averaging measurement scheme to increase the signal-to-noise ratio, the custom-developed scanning probes can also quantify the much lower thermal conductance of single-molecule junctions (**Figure 9**). It is important to point out that unlike electron-dominated heat transport in single metallic atomic junctions (where thermal conductance is in the ≈500 pW K^{-1} range), heat conduction through single molecule junctions is predominantly mediated by phonons, resulting a much smaller thermal conductance (tens of pW K^{-1}). The quantification of such a small thermal conductance, reported by Cui et al., was enabled by the combination of the C-SThM probes with excellent mechanical stability and thermal sensitivity and the time-averaging measurement scheme for noise reduction. Combining these two methods, they were able to achieve temperature resolution of ≈0.1 mK that enables detection of heat currents with ≈80 pW resolution, or thermal conductance with a resolution of ≈2 pW K^{-1} root mean square. In their experiments, electrical signal and thermal signal were simultaneously monitored, and the formation of a single Au–alkanedithiol–Au junction between the gold coated C-SThM probe, which was heated above ambient temperature, and the gold bottom surface, which is maintained at ambient temperature, was detected via its electrical conductance under a small external bias. Upon the trapping of a single molecule, the C-SThM probe was held in place to stabilize the junction until a sudden drop in electrical signal was observed, indicating the rupture of the junction, i.e., breakdown of thermal conduction pathway through the molecule. A small temperature rise on the probe side is expected to occur immediately after the rupture of the junction. However, change in the thermal conductance for a single molecule trapping event is not discernible due to resolution limit of the C-SThM probe (Figure 9c). By averaging hundreds of thermal conductance traces from single molecule trapping events, a clear thermal conductance drop upon junction breakdown was revealed (Figure 9d). They showed that the thermal conductance of single Au–alkanedithiol–Au junctions, where number of carbon atoms varies from two to ten, is independent of the molecular length (Figure 9e). The measured thermal conductance of these junctions is around 10–20 pW K^{-1}. This finding immediately clears the discrepancy in the molecular length dependence of thermal conductance in single alkane chains reported amongst previous theoretical studies. It is reasonable to expect that the experimental approach presented in this work will soon enable direct characterization of thermal conductance and thermoelectric figure of merit ZT of many other short molecules, polymer chains, and low-dimensional nanostructures.

3.2. Heat Dissipation and Local Heating/Cooling in MJ

At the macroscale, current flow through a standard resistor results in heating (Joule heating) because the inelastic electron–phonon interactions in the resistor which transfer energy to the surrounding lattice. In a nanoscale MJ, energy dissipation is governed by the nature of charge transport in the molecular region, i.e., it depends on whether the transport is inelastic or not. As described in Section 2, the Landauer approach can be used to explain heat dissipation of elastic (ballistic) transport in MJs where heat is mainly dissipated at the electrodes. However, it has remained challenging to model the inelastic processes, such as electron–phonon interactions in the molecular region. This is mainly because the small heat capacity of a molecule often leads to dramatic increase in the local kinetic energy of atoms even when a comparatively small amount of heat is dissipated in the molecular region.[13b] Given that the classical definition of temperature is for equilibrium systems, such nonequilibrium scenarios require redefining the local temperature in the molecular region. In this section, we will discuss the theoretical and experimental investigations of heat dissipation and local heating or cooling in MJs.

3.2.1. Theoretical Studies

Computational efforts have been devoted to understanding the physical mechanisms of energy dissipation in MJs induced by both elastic and inelastic processes. To account for heat dissipation in molecular junctions (mainly in the electrode region due to inelastic processes), Landauer's formalism is commonly employed. For example, by combining the Landauer approach with ab initio calculations, Zotti et al.[53] studied heat dissipation in short, single-molecule junctions based on benzene derivatives. Their calculations suggest that heat is mainly dissipated in the two electrodes, as expected from elastic transport, and the heating is intrinsically determined by the electronic structure of the molecule (**Figure 10**a). Specifically, heat is not equally dissipated in both electrodes (bias polarity dependent) and dissipation is intimately related to the thermopower of the junction (Figure 10b).

To understand the inelastic processes in the molecular region, Segal et al.[54] evaluated the fraction of available energy, i.e., the energy associated with the potential drop across the junction, that is released as heat on the molecular bridge. To characterize heating in the molecular region, it is important to consider two factors, the amount of electronic energy directly deposited on the molecule and the rate of heat conduction away from the molecule. Using their model, they found that the heating in the molecular region causes temperature rise to be ≈3 K. However, they argued that their approach employs an oversimplified classical heat conduction model which is expected to underestimate the heating effect. A unified description for the phonon thermal flux was later derived by Gelperin et al.[55] to define and quantify a local effective temperature in nonequilibrium systems, such as MJs. The molecular length dependence of local heating induced by electron–phonon scatterings was further studied by Chen et al.[56] in alkanethiol molecular chains. Assuming good thermal dissipation into the bulk electrodes, they found that the local temperature is smaller in longer chains (Figure 10d). They also show that the inelastic scattering profile displays an odd-even effect which is very sensitive to the structure of the carbon–sulfur–gold bond at the molecule–electrode interface.
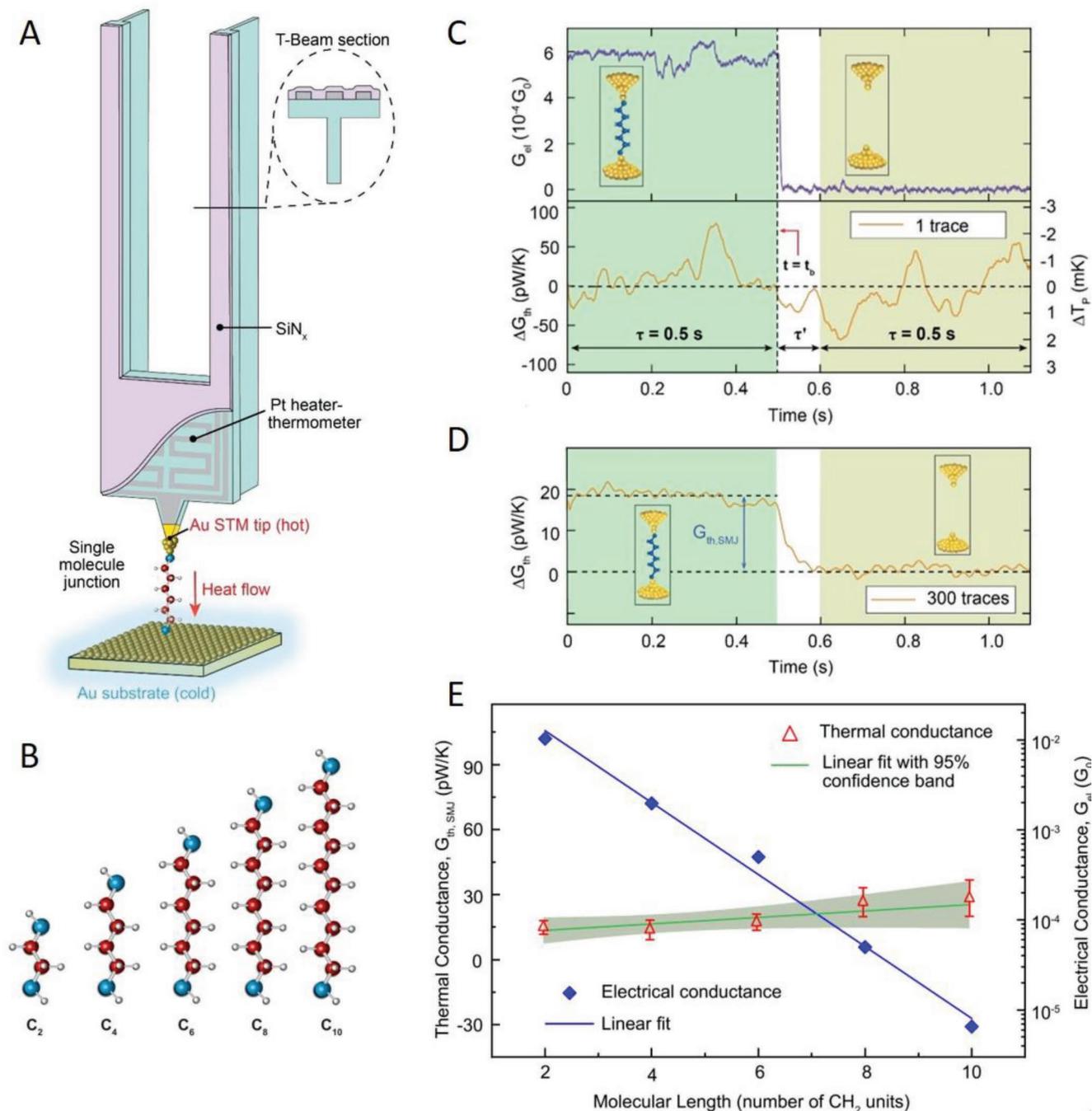
Figure 9. Thermal conductance measurements of single Au–alkanedithiol–Au molecular junctions. A) Schematic of the calorimetric scanning thermal microscopy (C-SThM) setup. A single molecule is trapped between a Au-coated tip of the C-SThM probe, which is heated to temperature (T_P) by inputting a heat current (Q) via an embedded Pt heater-thermometer, and a Au substrate at temperature (T_S) that is equal to ambient temperature (T_{amb}). B) Schematics of alkanedithiol molecules (C_n) studied in this work, $n = 2, 4, 6, 8, 10$ denotes the number of carbon atoms in the molecule. C) Experimental protocol for measuring the thermal conductance of a single-C_6 junction. The electrical conductance trace (upper panel) corresponds to the rupture (at $t = t_b$) of a single-molecule junction, indicated by a sudden drop of the measured electrical conductance G_{el} value. The thermal conductance change (ΔG_{th}, left axis) and the related temperature change of the probe (ΔT_P, right axis), where the small effects of Joule heating are already accounted for, are shown in the bottom panel. It can be seen that, unlike the clearly identifiable electrical conductance change associated with the breaking of the junction, the corresponding thermal conductance change is not discernible in the noisy signal. D) An improved signal-to-noise ratio is obtained upon aligning via G_{el} and averaging 300 thermal conductance traces. A clear thermal conductance drop can be seen after averaging. E) Measured electrical (blue square, right axis) and thermal conductance (red triangle, left axis) as a function of the molecular length, as given by the number of CH_2 units in the alkanedithiol junctions. The solid blue line indicates a linear fit to the electrical conductance data on a logarithmic scale. The measured thermal conductance data are fit by a linear curve (green line) on a linear scale, with the region shaded in light green representing the 95% confidence band. Error bars represent one standard deviation of the data. Reproduced with permission.[52] Copyright 2019, Springer Nature.
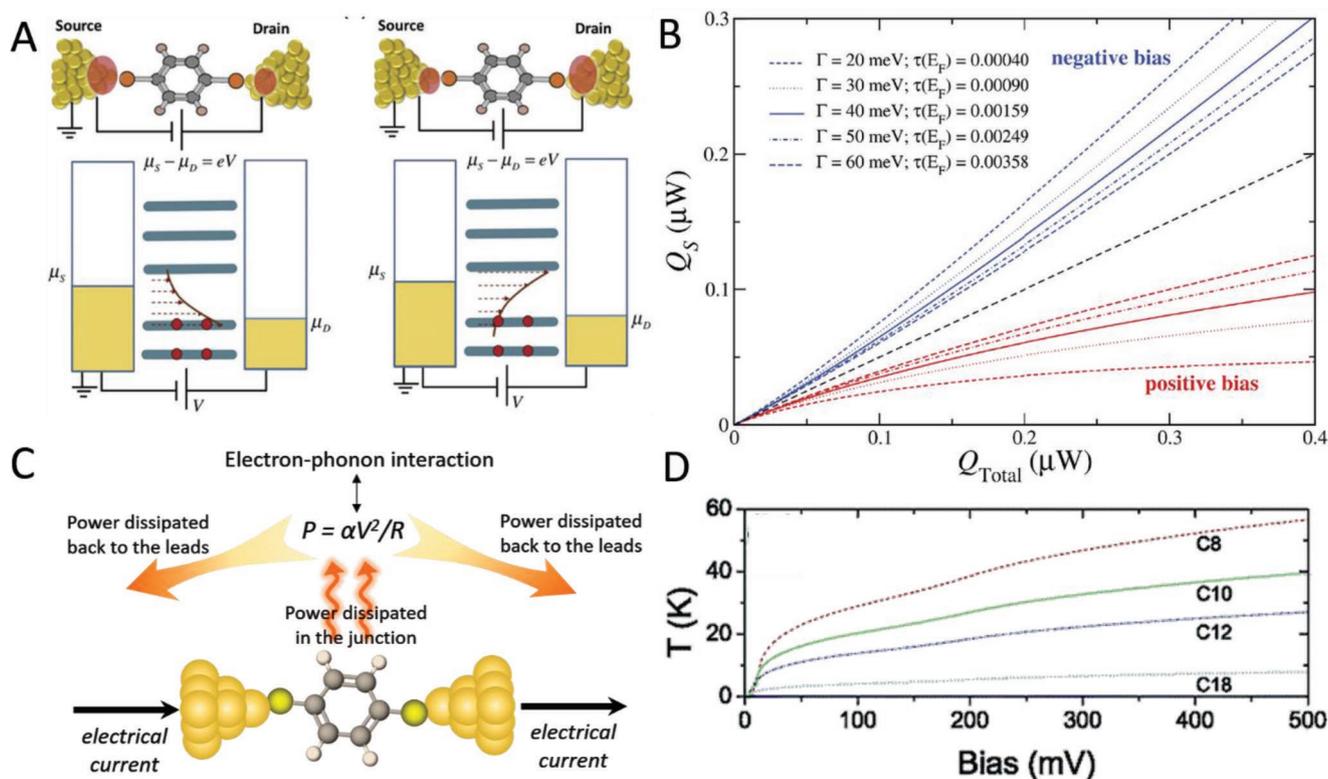
Figure 10. Theoretical computations of heat dissipation in molecular junctions. A) Landauer models of asymmetric heat dissipation in the electrodes of a molecular junction. The heat dissipation depends on the transmission function in the transmission window. B) Asymmetry of heat dissipation for different molecule–electrode coupling strengths. Q_{total} is the total heat dissipation and Q_s is the heat dissipated in the source electrode. A,B) Reproduced with permission.[53] Copyright 2014, Institute of Physics Publishing (IOP). C) Schematic of heat dissipation in the molecular region due to inelastic scattering. α is the fraction coefficient of heat dissipated in the molecular region out of the total heat dissipation. Reproduced with permission.[13b] Copyright 2011, American Physical Society. D) Local temperature rise T as a function of bias for alkanethiols with different lengths. Heat dissipation into the bulk electrodes is taken into account. Reproduced with permission.[56] Copyright 2005, American Chemical Society.

The electron current density in nanoscale junctions is typically several orders of magnitude larger than that in bulk electrodes. Consequently, the electron–electron scattering rate increases substantially in the junction, which leads to local electron heating. To account for the electron–electron scattering-induced heating, D' Agosta et al.[57] derived a model based on a hydrodynamic approach. Using their model, they found that the rate of electron–electron scattering could be comparable to that of electron–phonon scattering, suggesting that electron–electron scattering also plays an important role in determining the local temperature of the molecular bridge. In this context we note that heat dissipation in the molecular region is usually much smaller than the dissipation in the electrodes.

Given the possibility of taking advantage of cooling mechanisms for overcoming heating-induced instability or breakdown of molecular electronic devices, several groups have systematically explored this possibility.[58] For example, Galperin et al.[58a] demonstrated mechanisms of cooling in MJs under an applied bias. Specifically, they proposed two cooling mechanisms resulting from a) cooling of the high-voltage side of an MJ due to depletion of high-energy electrons and b) inelastic electron tunneling. The latter occurs when the available electronic energy is not sufficient for efficient transmission, the needed excess energy can be provided by absorbing phonons from the vibrational subsystems. Simine et al.[58c] studied

current-induced vibrational cooling in a donor–acceptor rectifying MJ and reported bias-induced cooling of the vibrational mode at relatively low bias voltages (<0.2 V). Recently, Lykkebo et al.[58d] provided strategies to enhance the inelastic absorption processes compared with the emission process in the molecular region to achieve cooling in MJ. Using their strategies, they demonstrated that under certain bias, the local temperature of the MJ can be effectively cooled to a temperature below ambient environment. Although the estimated cooling effect is small, the design strategies outlined in their study could aid in the rational design of local cooling in MJs.

3.2.2. Experimental Studies

Researchers have recently developed several experimental techniques to quantify energy dissipation, local heating, and cooling in current carrying molecular junctions. These techniques can largely be divided into two categories: 1) direct detection of temperature changes in MJ and 2) indirect determination of temperature by probing thermally activated processes such as junction lifetime. Given the lack of appropriate experimental approaches to directly measure temperature changes in the molecular region, initial studies relied on indirect approaches.[59] For example, Huang et al.[59a,c] used
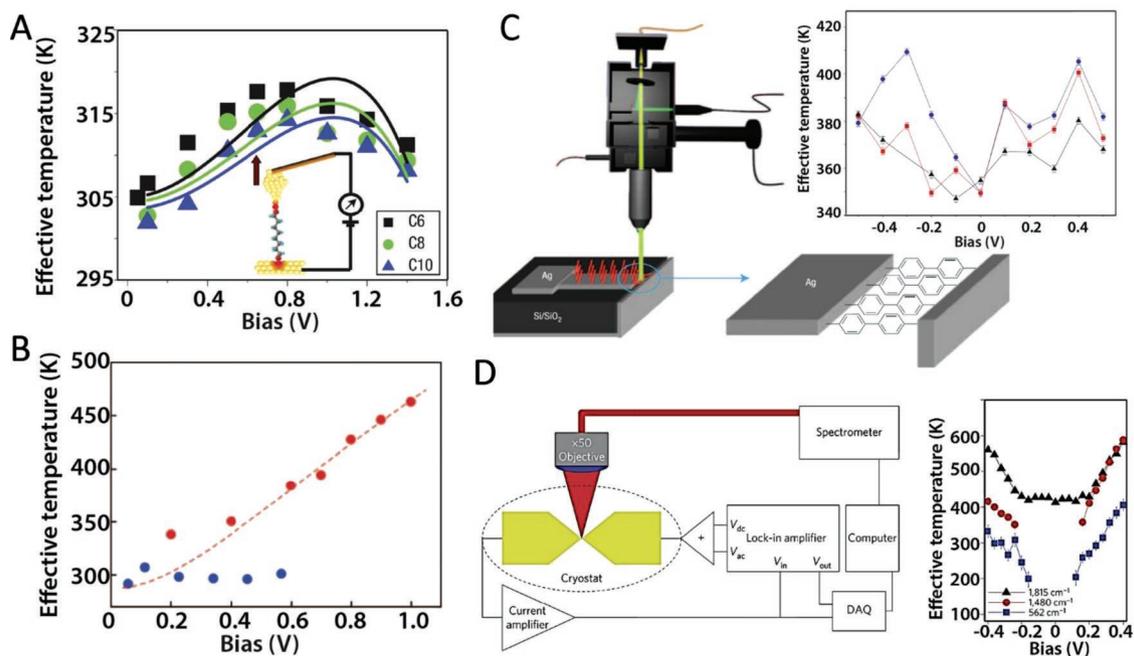
Figure 11. Experimental measurements of effective temperature of molecular junctions using indirect approaches. A) Effective temperature in alkanethiols molecular region as a function of bias. The effective temperature is estimated from the junction stretching length measured using STM-BJ technique. The solid lines are the fitting of the experimental data to a hydrodynamic theoretical model which includes both the electron–phonon and electron–electron interactions. Reproduced with permission.[59c] Copyright 2007, Springer Nature. B) Local temperature of benzenedithiol (red) molecular junction and Au (blue) atomic junction. The local temperature is estimated from measured junction lifetime. Reproduced with permission.[59b] Copyright 2008, American Chemical Society. C) Scheme of an "on-edge" junction under the Raman setup. Inset: Measured effective temperature as a function of bias voltage for biphenyldithiol (BPDT) molecular junctions. Reproduced with permission.[60] Copyright 2008, Springer Nature. D) Schematic of electrical and optical measurements with integrated SERS (left) and measured effective vibrational temperature as a function of bias voltage for three OPV3 modes (right): 1815 cm^{-1} (black), 1480 cm^{-1} (red), and 562 cm^{-1} (blue). Reproduced with permission.[61] Copyright 2011, Springer Nature.

scanning tunneling microscopy-based techniques to study current-induced local ionic heating effects (atomic vibrations in the molecular region of the junction that arise due to the interaction of atoms with current-carrying electrons is termed local ionic heating) in single molecules (6-, 8-, and 10-alkanedithiol) covalently attached to two gold electrodes as a function of applied bias and molecular length. They reasoned that the breakdown process is thermally activated and the effective temperature of the molecular junction can be related to the stretching distance of the junctions before breakdown. Specifically, from measuring the MJ stretching length before breakdown, they found that at a given bias, the local ionic heating increases with decreasing molecular length. Further, they claimed that for a given molecule, the effective local ionic temperature first increases with bias and then decreases after reaching a maximum value at ≈0.8 V due to electron–electron interactions and consequent local electron heating at the junction (**Figure 11**a). Taking advantage of the instability of MJs when subjected to a high electric field, Tsutsui et al.[59b] employed a mechanically controlled break junction (MCBJ) technique to estimate the local temperature of Au–benzenedithiol–Au junction by fitting junction lifetime to a model that related the applied bias and effective temperature to the junction lifetime. They estimated from their experiments that Au–benzenedithiol–Au junction heats up to ≈463 K under a bias of 1 V (Figure 11b).

Besides using break-junction techniques, Ioffe et al.[60] and Ward et al.[61] showed that surface-enhanced Raman

spectroscopy (SERS) can also be used to determine the effective temperatures for electrons in a biased MJ. In their studies, the temperature-dependent parameter is the anti-Stokes (AS)/Stokes (S) ratio, which is used to estimate the local temperature. Specifically, Ioffe et al. reported a temperature rise of the order ≈30 K in Ag–biphenyldithiol (BDT)–Ag junctions for both bias polarities (Figure 11c). Ward et al.[61] characterized the electronic temperature of a three-ring oligophenylene vinylene (OPV3) MJ and observed a pronounced temperature rise of 200–300 K under applied bias of 0.4 V (Figure 11d). These studies highlight the potential of SERS as a temperature sensing technique at the molecular level.

Direct experimental quantification of heat dissipation in single molecule junctions was inaccessible until a recent work by Lee et al.[24] who employed custom-fabricated scanning tunneling microscope (STM) probes with integrated nanoscale thermocouples in an STM break-junction setup (**Figure 12**). In their work, the temperature change of the STM probe due to heat dissipation was detected by nanoscale thermocouples integrated in the probe. They identified asymmetric heat dissipation, that is, unequal dissipation on the two electrodes, in the molecular junctions formed with benzenediisonitrile (BDNC) and benzenediamine (BDA) molecules. Combining experimental results and first principle calculations, they showed that the heat dissipation is dependent on both the bias polarities and the identity of the majority charge carriers (electrons vs holes) and its asymmetry is directly associated with the
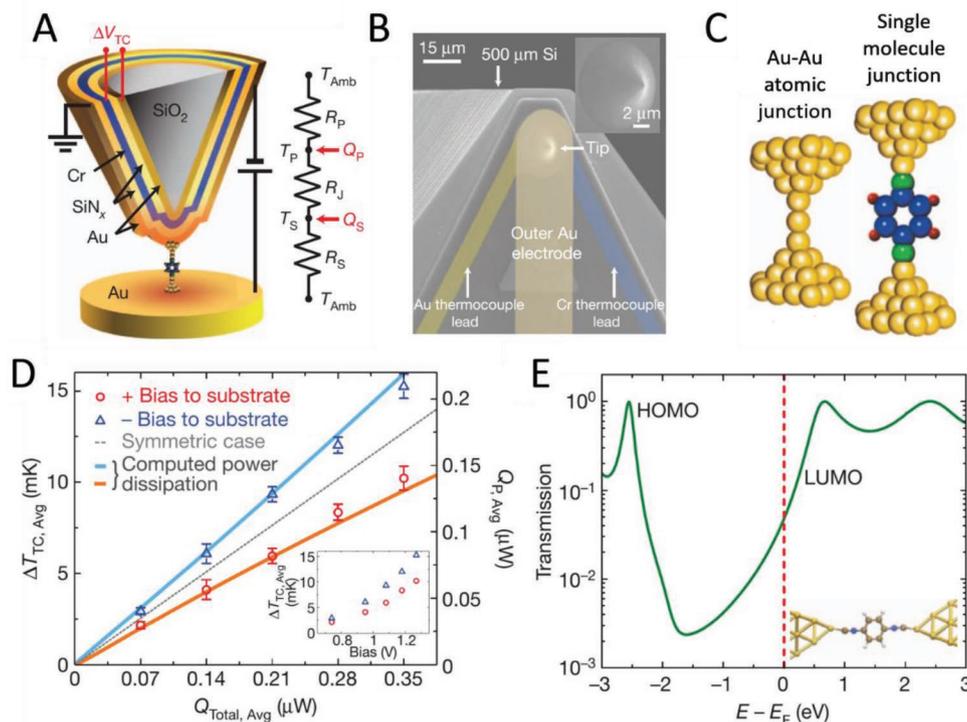
Figure 12. Direct measurement of heat dissipation in single molecule junctions. A) Schematic of a molecular junction created between a nanoscale thermocouple probe (cross-section view) and a Au substrate. B) Scanning electron microscopy (SEM) image of the nanoscale thermocouple probe. C) Schematics of a Au–Au atomic junction and a single-molecule junction. D) Measured time-averaged temperature rise ($\Delta T_{TC,Avg}$) of the thermocouple probe versus the time-averaged power dissipation ($Q_{Total,Avg}$) in the probe under different bias polarities for Au–benzenediisonitrile (BDNC)–Au junction. Inset: Measured $\Delta T_{TC,Avg}$ as a function of applied bias. E) Calculated zero-voltage transmission function of Au–BDNC–Au junction. Reproduced with permission.[24] Copyright 2013, Springer Nature.

electronic transmission characteristics, i.e., the sign and magnitude of the Seebeck coefficient of the MJs.

In another recent work, Cui et al.[15b] employed a conductive atomic force microscope (AFM) setup in conjunction with custom-fabricated calorimeters[62] to directly quantify cooling in MJs due to Peltier effect. Based on the Landauer theory, for small applied biases, when the applied bias V is smaller than $2|ST|$ (where S is the Seebeck coefficient of MJ and T is the environment temperature), one expects to observe Peltier cooling when SV, the product of the Seebeck coefficient and the applied bias, is negative. To probe such an effect, Cui et al.[15b] developed a custom-fabricated, calorimetric microdevice that serves as the substrate electrode in their AFM-based measurement scheme, which enables measurement of heating or cooling with ≈30 pW resolution (**Figure 13**). Using this setup, they observed for the first time cooling due to the Peltier effect in SAM junctions consisting of either 4,4′-dibenzenedithiol (DBDT), 4,4′-tribenzenedithiol (TBDT), and 4,4-bipyridine molecules at a small applied bias (see Figure 13 c,d). They showed that the maximum cooling occurred at different applied biases for different molecules and that it is directly related to the transmission characteristics of the studied molecules. Finally, it is to be noted that this work also demonstrated that it is possible to directly measure electrical and thermoelectric transport properties on the same MJ in a unified manner. Specifically, they concluded that by combining calorimetric tools with scanning probe techniques it is possible to obtain

important insights into energy conversion, dissipation, and transport in MJs.

We note that while some of the experiments discussed above focused on resolving heat dissipation (temperature rise) in the molecular region others focused on studying heat dissipation in the electrodes of the MJ. These two aspects do not necessarily contradict each other because the total power, that is, the product of the current and applied voltage, must be dissipated in either the molecular region or in the electrodes. In general, for short MJs, given that electron transport across the molecule is largely elastic, most of heat is deposited on the electrodes. However, due to the relatively small heat capacity of a molecule, even a tiny amount of dissipation in the molecular region could induce a significant increase in the local temperature.

4. Thermoelectric Properties of Molecular Junctions

Thermoelectric materials convert heat to electricity, enabling applications in energy conversion and solid-state cooling. The usefulness of a thermoelectric material is determined by two factors: device efficiency (i.e., the figure of merit, ZT) and power factor ($G_e S^2$, where G_e and S are the electrical conductance and Seebeck coefficient of the material). Many studies have suggested that molecular-scale thermoelectric materials hold great
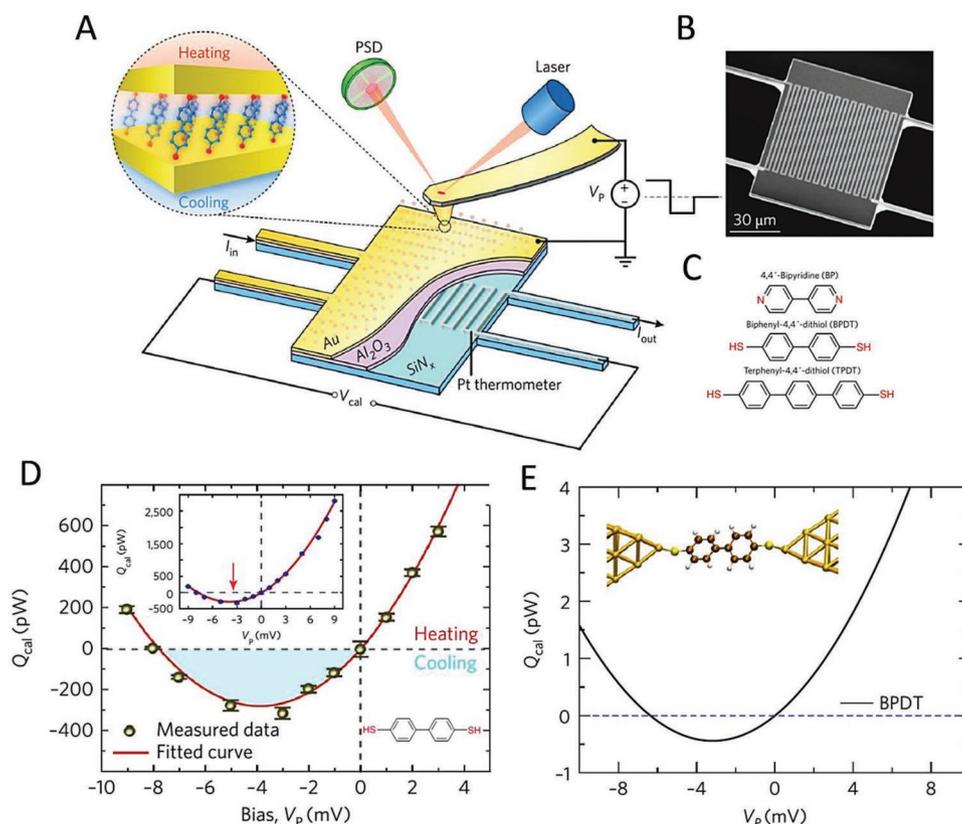
Figure 13. Experimental demonstration of Peltier cooling in molecular junctions. A) Schematic of the SAM molecular junctions created by placing a Au-coated AFM probe in contact with an SAM formed on a Au-coated calorimetric microdevice. B) SEM image of the calorimetric microdevice. C) Chemical structures of the molecules studied. D) Measured voltage dependent thermal power for biphenyldithiol (BPDT) junctions. Shaded blue region indicates the net cooling (refrigeration) observed. Inset: Full range data from −9 to 9 mV. E) Calculated heating and cooling power at different voltages for BPDT. Reproduced with permission.[15b] Copyright 2018, Springer Nature.

promise for improving device performance and creating properties that are not possible with bulk materials.[13a,c] This research topic has therefore received continuously growing attention in recent years. In this section, we discuss recent advances in probing thermoelectric properties of MJs, including theoretical computations and experimental observations.

4.1. Theoretical Studies

The first theoretical study of thermoelectric voltage of an MJ was performed by Paulsson et al. in 2003.[12] Their computational results suggested that the thermoelectric voltage of a BDT MJ is in principle measurable and somewhat insensitive to the molecule–electrode coupling at the contacts. It is necessary to note that later theoretical and experimental investigations found that the molecule–electrode coupling has a measurable impact on the thermopower of molecular junctions. Nevertheless, this first theoretical work indicated that measuring thermoelectric voltage of molecular junctions provides valuable information on the location of electrode Fermi level relative to the frontier molecular orbitals. Similarly, Segal et al.[63] also suggested that thermopower measurements can complement standard $I-V$ experiments with the advantage of their insensitivity to the metal–molecule contact. Stimulated by these early works and

with the excitement of molecular-based thermoelectricity applications, extensive efforts have been devoted to probe the thermopower and figure of merit ZT of MJ systems and seeking strategies to enhance device efficiency. We note that due to technical difficulties in direct experimental quantification of single molecule thermal conductance, the figure of merit ZT of a single molecule junction has remained experimentally inaccessible so far. Therefore, the ZT values of single molecule junctions discussed in this section are often based on computed results of the thermal conductance and may need to be reevaluated in the future if experimental techniques for thermal measurements become available.

Theoretical simulations have shown that molecular length, contact chemistry and molecular orientation have significant impact on the thermoelectric properties of MJs. For example, using an ab initio method, Huser et al.[64] calculated the Seebeck coefficient of MJs featuring small saturated and conjugated molecular chains (alkane, alkene, and alkyne chains) of varying length wired to gold electrodes via different binding groups (−SH, −NC, and NH₂). They found that for alkane chains, the thermopower increases roughly linearly with length for all binding groups. The onset (the thermopower at zero molecular length based on a linear fit to the calculated thermopowers at different lengths), however, is very different for the four binding groups, resulting in positive

**ADVANCED
SCIENCE NEWS**
www.advancedsciencenews.com

**ADVANCED
FUNCTIONAL
MATERIALS**
www.afm-journal.de

and increasing thermopower for −SH and negative and increasing thermopower for −NC. For −NH$_2$, the thermopower changes sign with increasing length. For alkene chains, the calculated thermopower for −NH$_2$ linker is small and has no linear dependence on molecular length. A different situation occurs for alkene with −NC linker: the thermopower has a large negative onset and decreases even more with length. The thermopower for alkene with −SH linker is again positive and increasing. For alkyne chains, several different length dependence scenarios are observed: positive and increasing (−SH), negative and decreasing (−NC), and changing sign from positive to negative (−NH$_2$). Clearly, a simple assumption that the thermopower depends linearly on the length and that this dependence is given by the nature of molecular backbone does not hold. In fact, this work points out that transmission resonances near Fermi level, in particular the position and shape of the resonances, not only determine the contact Seebeck coefficient but also can have a large influence on the length-dependence itself, suggesting that it is theoretically difficult to separate the end group from backbone effects. In another study, using a combination of DFT and tight-binding calculations, Vacek et al.[65] demonstrated that stretching or compressing a helicene molecule can dramatically change the electronic properties of the helicene, leading to a tunable switching behavior of the electrical conductance and Seebeck coefficient of the junction with on/off ratios of several orders of magnitude. They also showed that varying the helicene length and number of rings leads to more than an order of magnitude increase in both the Seebeck coefficient and figure of merit, which is mainly due to a shift in the position of frontier molecular orbitals.

Recently, Manrique et al.[66] studied a general rule for coherent quantum transport (electrical conductance and Seebeck coefficient) in MJs by investigating a large set of molecules with symmetric and asymmetric anchor groups. As shown in **Figure 14**, the molecules examined by this group have a structure of X–B–Y, where B is the backbone of the molecule, while X and Y are anchor groups. Assuming that transport takes place via coherent tunneling and that inelastic effects are negligible, their rule states that the conductance G_{XY} of an asymmetric molecule is the geometric mean $\sqrt{G_{XX}G_{YY}}$ of the conductance of the two symmetric molecules, and the thermopower S_{XY} of the asymmetric molecule is the algebraic mean $(S_{XX} + S_{YY})/2$ of their thermopowers. Applying this prediction to existing experimental results of conductance and Seebeck coefficient, they show that this rule agrees with the statistically most probable values, suggesting it as a good first estimate for the transport properties of unmeasured MJs.
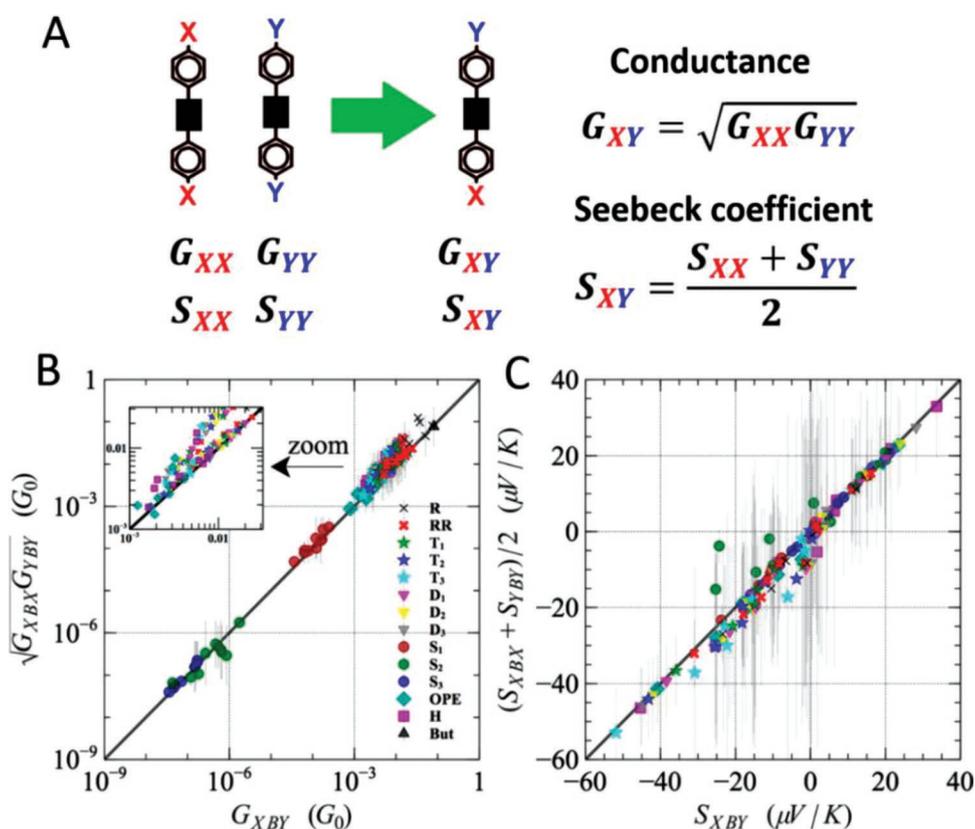

Figure 14. A general circuit rule for estimating the electrical conductance and thermopower of molecular junctions in an X–B–Y motif, where B is molecular core, and X and Y are the chemical anchor groups. A) Mathematical description of the rule: The conductance of G_{XBY} of an asymmetric molecule is the geometric mean of the conductance of the two symmetric molecules. The thermopower S_{XBY} of the asymmetric molecule is the algebraic mean of the thermopowers of the two symmetric molecules. B) Comparison between the electrical conductance G_{XBY} and geometric means $(G_{XBX}G_{YBY})^{1/2}$ for different molecules. C) Comparison between the thermopowers S_{XBY} and the arithmetic means $(S_{XBX} + S_{YBY})/2$ for different molecules. Reproduced with permission.[66] Copyright 2015, American Chemical Society.
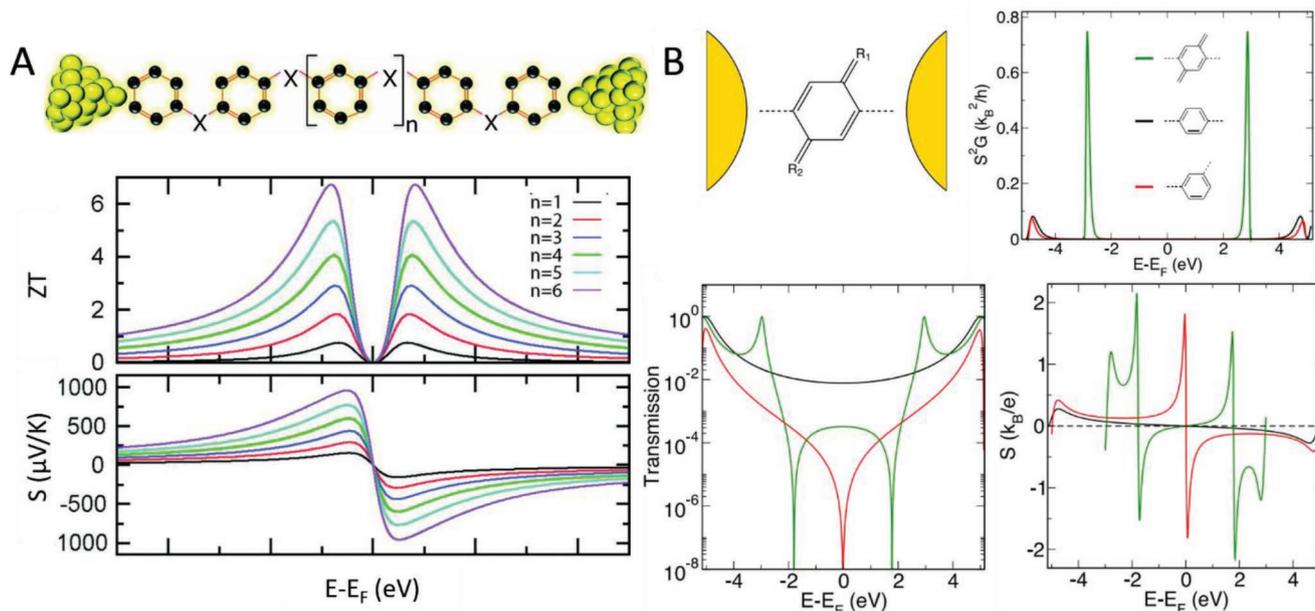
Figure 15. Calculated quantum interference effect on thermoelectric transport in molecular junctions. A) Calculated supernode enhancement of *ZT* and thermopower *S* for polyphenyl ether (PPE) molecular junctions with n repeated phenyl groups, shown schematically above the top panel. Reproduced with permission.[14a] Copyright 2010, American Chemical Society. B) Upper left: Schematic of a quinoid molecule sandwiched between metal leads. Upper right: Power factors $G_e S^2$ for a quinoid structure (green) and benzene connected in *ortho* (black) and *meta* (red) position. Lower left: Transmission function of the molecules. Lower right: Thermopower of the molecules. Reproduced with permission.[69] Copyright 2015, AIP Publishing.

In addition to the above described phenomena, bithermo-electricity effects in MJs, that is, coexistence or sign switching of positive and negative Seebeck coefficients of the same MJ, have also been recently reported. For example, Stuyver et al.[67] recently explored the theoretical design of reversible bithermo-electric switches, molecules which can be switched reversibly between a positive and negative Seebeck coefficient through the application of external stimuli. They studied heptaphyrins, a class of expanded porphyrins that can be shifted between a Hückel and Möbius topology. It was suggested that these molecules can switch between the two π-conjugation topologies, causing the thermopower to change considerably from +50 to −40 µV K^{-1}, respectively. In another work, Sangtarash et al.[68] studied the dependence of connection points at which electrons are injected into and collected from a molecule on the thermo-power of a group of polycyclic aromatic hydrocarbons (PAHs). They showed that by carefully choosing different heteroatoms and connectivity, the energy shift of antiresonance can be controlled to be above or below the Fermi energy, thereby creating MJ devices with negative or positive Seebeck coefficients.

A major focus of theoretical investigations on thermoelectric properties of MJ has been to explore the possibility of achieving high *ZT* in MJs. Toward this goal, several strategies have been theoretically proposed. Among the proposed approaches, harnessing QI effects in MJs have been considered as one of most promising methods.[19b] For example, Bergfield et al.[14a] showed that higher order QI features in the transmission spectrum of polyphenyl ether (PPE) MJs containing *n* repeated phenyl groups give rise to giant enhancement in thermoelectric performance (**Figure 15**a). Specially, the figure of merit *ZT* was suggested to scale linearly with *n*, exhibiting a peak value of 6.86 for *n* = 6, and the Seebeck coefficient *S* is also enhanced with

a peak value of 957 µV K^{-1} for the same value of *n*. In another work, using DFT method, Strange et al.[69] investigated a series of molecules featuring a quinoid core and showed that these molecules have two distinct destructive QI features close to the frontier orbital energies (Figure 15b). These QI features, mani-fested as two dips in the transmission function, result in a very high thermoelectric power factor $G_e S^2$ and figure of merit *ZT*. They further demonstrated that these features can be controlled by varying the electron donating or withdrawing character of the side groups as well as the conjugation length of the molecule.

Other strategies to enhance the thermopower and *ZT* include carefully controlling the molecular orientation, chemical struc-ture, and electrode materials of the MJ. For example, Finch et al.[14b] reported that controlling the angular orientation of the side group of a CSW-479-bipyridine molecule leads to crea-tion of Fano resonance effect (**Figure 16**a). This effect, mani-fested as sharp transmission peak near the Fermi level, results in great enhancement in both the thermopower and *ZT*. To improve the maximum thermoelectric power and the efficiency at maximum power, Karlstrom et al.[70] show that it is possible to suppress parasitic charge flow near the Fermi energy and reduce electronic heat conduction by carefully engineering elec-tron quantum interference of a two-level system. They studied a prototype Au–Zn porphyrin–Au molecular junction with two almost-degenerate energy levels E_1 and E_2 both located close to and on the same side of E_F. They found that when the coupling strengths of E_1 and E_2 to the electrodes differ by a factor of a^2, the transmission function vanishes at E_F while maintaining a large value for a finite energy window above E_F. Such feature of the transmission function leads to a large gradient at E_F and finite energy width for electron transport. They further demon-strate such transmission system can operate with large power
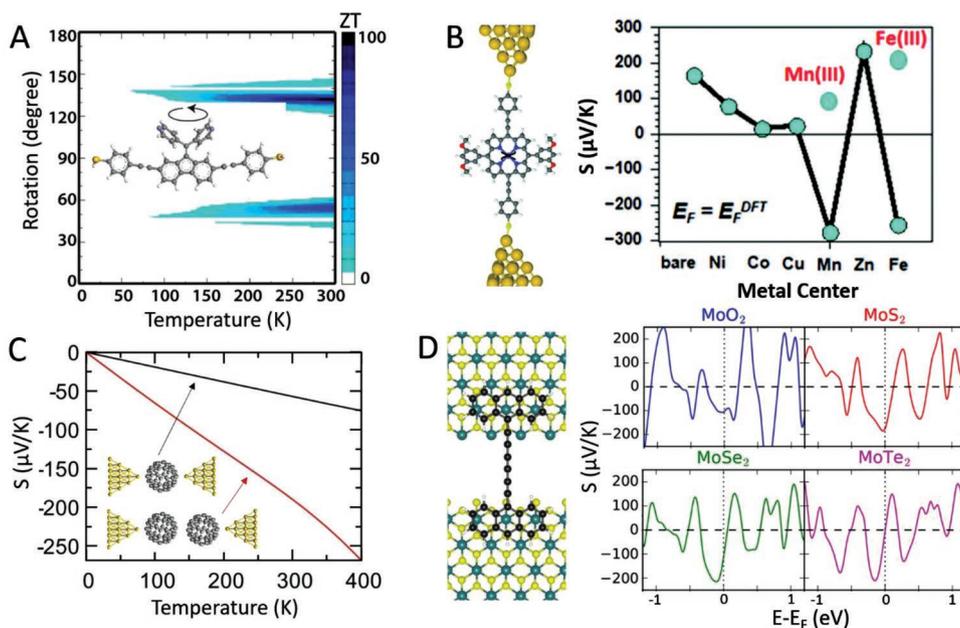
**ADVANCED
SCIENCE NEWS**

www.advancedsciencenews.com

**ADVANCED
FUNCTIONAL
MATERIALS**

www.afm-journal.de

Figure 16. Theoretical proposals for tuning thermoelectric transport in molecular junctions. A) Calculated *ZT* of CSW-479-bipyridine molecule as a function of temperature and rotation angle of the side group relative to the C—C bond connecting it to the molecule. Reproduced with permission.[14b] Copyright 2009, American Physical Society. B) Calculated Seebeck coefficient of porphyrin molecules with different metal centers. Reproduced with permission.[72] Copyright 2016, Royal Society of Chemistry. C) Calculated thermopower of the C60 monomer (black) and C60 dimer (red) junctions as a function of temperature. Inset: Schematic of C60 monomer and dimer junctions. Reproduced with permission.[22] Copyright 2017, American Physical Society. D) Calculated thermopower of a six-carbon alkyne chain molecule attached to two semi-infinite MoX_2 (X = O, S, Se, Te) 2D transition-metal dichalcogenides electrodes via the van der Waals forces. Reproduced with permission.[73] Copyright 2018, American Chemical Society.

output and efficiencies close to the Curzon–Ahlborn limit. Noori et al.[71] recently investigated the influence of metal ions on the thermoelectric properties of flat-stacked 5,15-diphenyl-porphyrins containing divalent metal ions Ni, Co, Cu or Zn. Their calculations show that changing the metal atom has little effect on the thermal conductance due to the phonons, while the room-temperature Seebeck coefficients of these junctions are high, ranging from 90 µV K^{-1} for Cu, Ni, and Zn-porphyrins to −16 µV K^{-1} for Co-porphyrin. The figure of merit *ZT* of these junctions ranges from 1.6 for Cu porphyrin to ≈0.02 for Ni-porphyrin. In another study, Al-Galiby et al.[72] presented calculations that showed that the thermopowers of porphyrin molecules with Mn(II) or Fe(II) metal centers are negative and lie in the range −280 to −260 µV K^{-1}. They also found that complexing them with Fe(III) and Mn(III) as counter anion changes both the sign and magnitude of the respective thermopower to +218 and +95 µV K^{-1} (Figure 16b). Besides, Klockner et al.[22] studied the thermoelectric properties of MJs with either a C60 monomer or a C60 dimer connected to gold electrodes (Figure 16c). They found that while stacking two C60 molecules to form a dimer molecule increases the thermopower of the MJ, phonon transport completely dominates the thermal conductance in dimer junctions and therefore reduces the figure of merit as compared to monomer junctions. More recently, Jin et al.[73] adopted the emerging 2D transition-metal dichalcogenides (MoO_2, MoS_2, $MoSe_2$, and $MoTe_2$) as the electrode materials and investigated the influence of these 2D materials on the MJ thermoelectric transport (Figure 16d). Their calculations reveal that the work function of these 2D materials can be tuned across the entire molecular energy range at a relatively

low bias with the appropriate choice of electrode material. Specially, by using van der Waals contacts between a molecular system (a six-carbon alkyne chain) with anthracene linker groups and the 2D transition-metal dichalcogenides electrodes, they found that the phonon contribution to heat transport can be effectively suppressed while achieving high levels of electron transport and thermopower as the molecular level is tuned into near resonance. This suggests a promising strategy to enhance thermoelectric performance of MJs.

The spin states of electrons have also been exploited to tune the thermoelectric properties of MJs. Along this line, Wang et al.[74] studied the spin-dependent thermoelectric transport through a magnetic molecule. Specifically, they found that the intrinsic magnetic anisotropy of single molecule magnet (SMM) can lead to oscillations of charge thermopower with gate voltage and a large violation of the Wiedeman–Franz law. It was also found that the spin-Seebeck coefficient in SMMs can be greater than the charge-Seebeck coefficient, and even a pure spin thermopower can be obtained accompanied by the charge thermopower vanishing. Furthermore, Ghosh et al.[75] recently computed thermoelectric transport across a spin-cross-over molecule (i.e., iron complex of 2-(1H-pyrazol-1-yl)-6-(1H-tetrazol-5-yl)pyridine). They showed that the spin-crossover process, that is, transition from low-spin state to high-spin state with the increase of temperature, can modulate the thermoelectric entities. They observed an increase in thermocurrent by four orders of magnitude and *ZT* enhancement by four times upon spin-crossover.

Taken together, theoretical studies have suggested that it is possible to achieve high-efficiency thermoelectric energy

ADVANCED
SCIENCE NEWS
www.advancedsciencenews.com

ADVANCED
FUNCTIONAL
MATERIALS
www.afm-journal.de

conversion (i.e., high thermopower and ZT) in MJs. The thermoelectric performance can be enhanced or controlled in various ways, including quantum interference effect, molecular structure and orientation, molecule–electrode contacts, and spin effects. However, to test the validity of these theoretical proposals, experimental techniques that are capable of simultaneously quantifying electrical conductance, thermopower and thermal conductance of MJ are urgently needed. So far, despite that electrical conductance and thermopower measurements in MJs have become routine, the thermal conductance of single MJs has remained challenging due to limited thermal resolution for existing temperature sensing techniques. In what follows, we discuss recent advances in experimental investigations of thermoelectric properties of MJs with special focus on the measurement of thermopower of MJs.

4.2. Experimental Studies

4.2.1. Experimental Methods

Direct experimental characterization of the thermoelectric properties of an MJ requires measurement of the thermovoltage induced by the temperature difference at the two terminals of the junction. When a temperature difference is established across the junction, this thermovoltage can be obtained in three ways: 1) Direct measurement of the voltage across the junction (thermovoltage) in an open-circuit configuration;[76] 2) Measurement of the junction current at zero external bias followed by conversion to thermovoltage using the electrical conductance of the junction.[77] 3) Measurement of the junction $I–V$ characteristics followed by analyzing the voltage offset at zero current, i.e., the voltage necessary to suppress the current).[78]

The experimental techniques employed to measure the thermopower of MJs were derived from those developed to probe

their electrical properties because the electrical signals (i.e., current or conductance) of the junction are usually leveraged as signature of the formation of an MJ. The circuit diagram and experimental schematics of commonly used techniques are illustrated in **Figure 17**. To measure the thermopower of a single molecule connected between two metal electrodes, researchers have employed STM break junction (STM-BJ),[76,79] MCBJ,[80] and electromigrated break junction (EMBJ)[6b] based approaches. Thermopower or the thermovoltage at a given temperature difference of a molecular junction is independent of the number of molecules participating in a molecular junction. This can be understood by considering N identical molecules in parallel in a junction. Assuming the interference effects are negligible, the total transmission τ of the junction will be $\tau_N = N\tau_1$, where τ_1 is the transmission of one molecule, applying Equation (5), one could obtain the thermopower of the junction $S_N = S_1$, where S_1 is the thermopower of a single molecule. Given that the thermovoltage is independent of the number of parallel molecules in the junction, conductive atomic force microscope (C-AFM) technique, which creates monolayer junctions that consist of many molecules in a junctions, and nanoparticle array method, which forms networks of MJs, have also been used for thermopower measurements.[81]

It is important to note that the formation of the junction can be either dynamic or static, depending on the specific technique chosen. For example, STM-BJ, MCBJ, and C-AFM techniques facilitate dynamic formation of the junction. The measurements using these techniques often rely on repeated formation of the junction and the following data processing is heavily statistical. Whereas, the EMBJ and nanoparticle array-based techniques involve nanofabrication of the junction and the measurement is performed in a static manner. While MJs formed by STM-BJ, C-AFM, and MCBJ techniques are typically two-terminal devices, a third gate electrode can be incorporated in an EMBJ setup to form three-terminal structure for
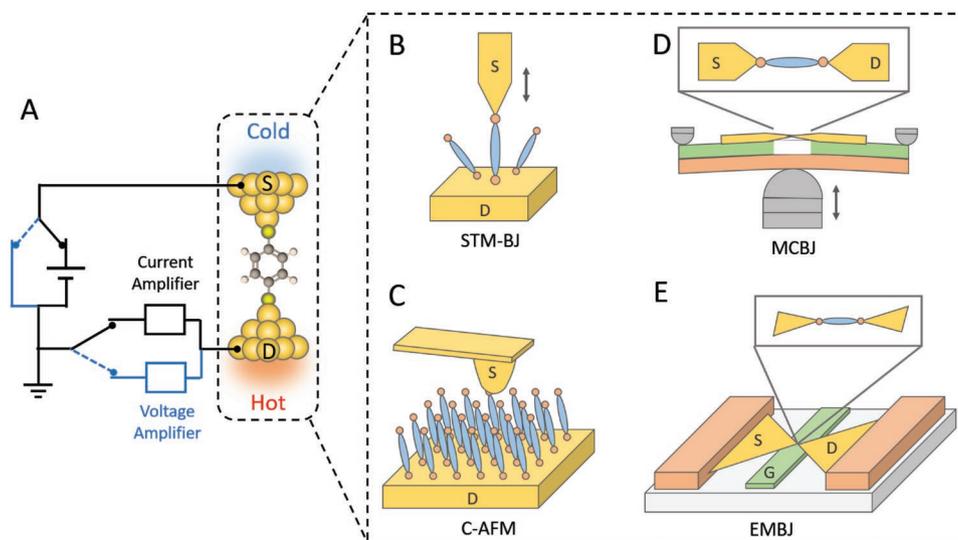

Figure 17. Representative experimental techniques for thermopower measurement in molecular junctions. A) Circuit diagram for thermopower measurement. B) Schematic of scanning tunneling microscope break junction (STM-BJ) based setup. C) Schematic of conductive atomic force microscope (C-AFM) based setup. D) Schematic of mechanically controlled break junction (MCBJ) based setup. E) Schematic of electromigrated break junction (EMBJ) based setup with a back gate integrated.

molecular orbital gating. More details about these techniques can be found in other literature.[1a,13c] In the following, we will discuss key insights obtained using the abovementioned techniques.

4.2.2. Experimental Results

The first measurement of the thermopower of MJs was reported in 2007 by Reddy et al.[76] The measurement was performed under ambient conditions by modifying the STM-BJ technique, which was first reported by Ruitenbeek's group[82] to measure electrical conductance of atomic wires and further developed by Xu and Tao[83] for studying the electrical properties of MJs. Specifically, a temperature difference ΔT is established between the Au STM tip and a Au substrate by heating the substrate while maintaining the tip temperature close to ambient. To measure the thermovoltage of the junction, they switched between a standard STM current mode, where a current amplifier was used to measure the current flow through the junction under an external bias, and the voltage mode, where a voltage amplifier is used to measure the voltage across the junction under zero external bias (**Figure 18**a). In the current mode, the STM tip approaches the substrate until the current signal reaches a preset setpoint, indicating the formation of MJs. Then, the external bias is immediately turned off and the measurement switches to the voltage mode to record the junction's thermovoltage which is brought about by the temperature difference ΔT across the MJ. Upon tip retraction, the thermovoltage versus

tip distance curve shows a steady thermovoltage signal until the last junction breaks, indicated by a sudden vanish of the voltage signal. The junction Seebeck coefficient is then obtained by measuring the thermovoltage of the MJ under different ΔT (Figure 18c). Their measurement results show that the room temperature Seebeck coefficients of 1,4-benzenedithiol (BDT), DBDT, and TBDT covalently bonded to Au electrodes are 8.7 (±2.1), 12.9 (±2.2), and 14.2 (±3.2) μV K^{-1}, respectively (Figure 18d). More importantly, the positive sign of the Seebeck coefficient unambiguously indicates hole (p-type or HOMO) conduction in these MJs, which was not accessible with other electrical measurements.

To avoid switching between the current mode and voltage mode, Widawsky et al.[84] modified the STM-BJ technique by directly measuring the thermocurrent of the junction under zero external bias. The thermovoltage is then obtained by dividing the thermocurrent with the electrical conductance measured for the same junction. This method enables simultaneous characterization of the electrical conductance and thermopower of the same MJ. Using this approach, they showed that the Seebeck coefficient is negative for pyridine–Au linked junctions, confirming the electron (n-type or LUMO) conduction mechanism, and positive for amine–Au linked junctions, confirming the hole (p-type or HOMO) conduction mechanism.

Thermopower measurement from junctions featuring multiple molecules was performed by Tan et al.[81a] In their study, a Au coated conducting AFM probe was brought into contact with a monolayer of molecules covalently bonded to Au substrate. The thermovoltage was directly measured using a
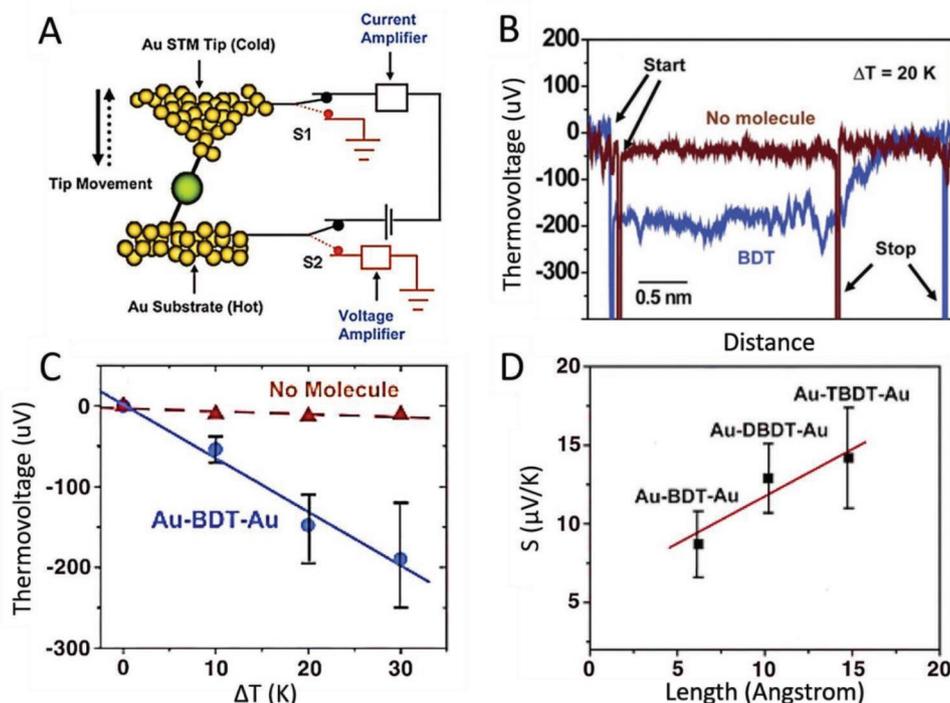

Figure 18. First thermopower measurement in molecular junctions by Reddy et al. A) Schematic of the experimental setup based on STM-BJ technique. B) Plot of the measured thermovoltage as a function of tip-sample distance. C) Plot of thermovoltage as a function of the temperature differential ΔT for Au–benzenedithol (BDT)–Au junction. D) Measured junction Seebeck coefficient S as a function of molecular length for BDT, DBDT, and TBDT. Reproduced with permission.[76] Copyright 2007, American Association for the Advancement of Science.
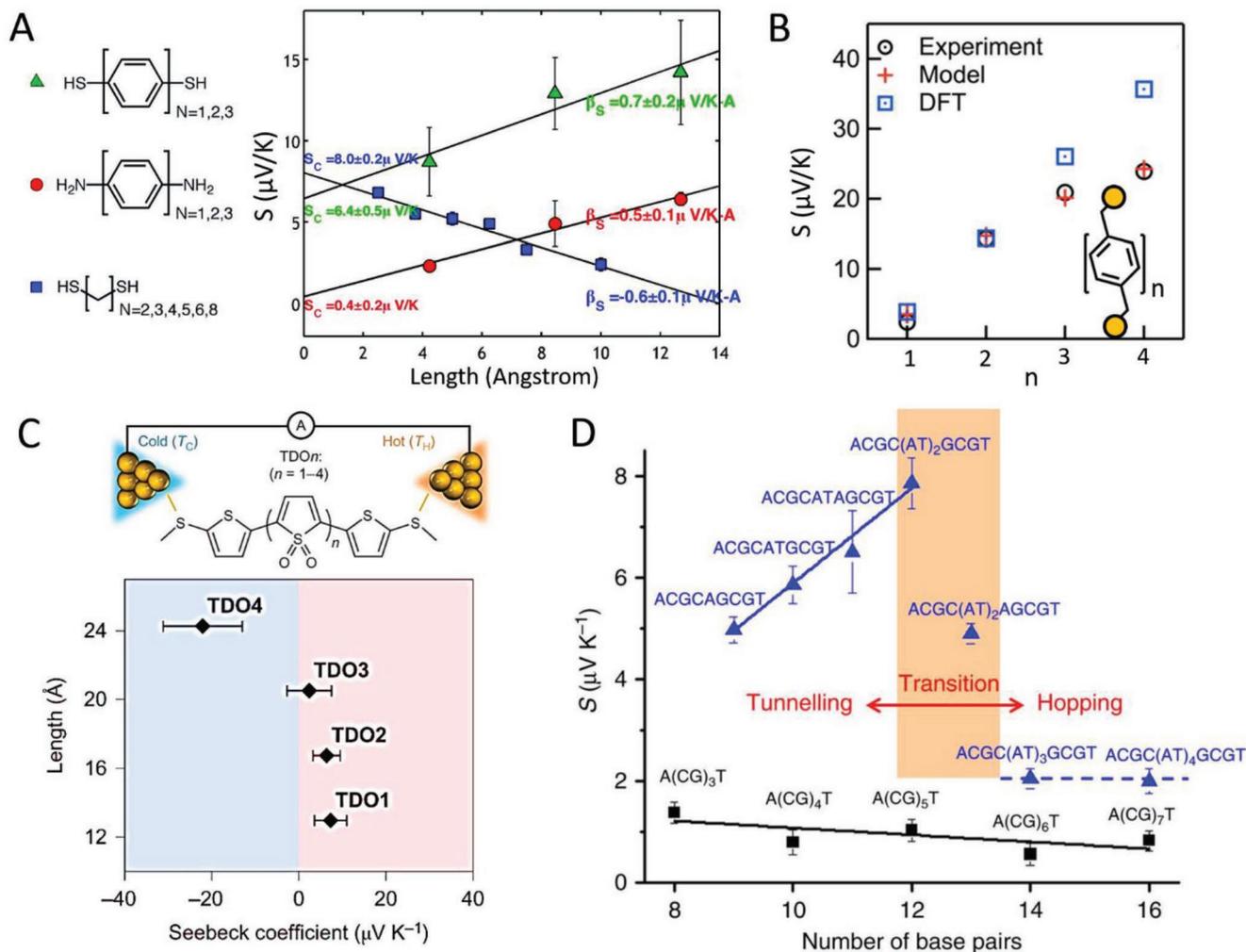
Figure 19. Experimental measurements of thermopower as a function of molecular length. A) Measured thermopower S as a function of molecular length for N-unit phenylenedithiols, phenylenediamines, and alkanedithiols. Reproduced with permission.[79] Copyright 2009, American Chemical Society. B) Thermopower determined from experiment, tight-binding model, and DFT as a function of the number of phenyl units for junctions with Au—C bond. Reproduced with permission.[77] Copyright 2013, American Chemical Society. C) Measured thermopower S as a function of molecular length for Au–oligothiophene–1,1-dioxide(TDO)$_n$–Au junctions. Reproduced with permission.[85] Copyright 2015, Springer Nature. D) Measured thermopower versus molecular length for single DNA molecules with different sequences. Reproduced with permission.[78] Copyright 2016, Springer Nature.

voltage amplifier upon formation of large number of junctions. The junction formation is predetermined by the current across the junction. This technique therefore still requires switching between the current mode and voltage mode. In order to measure the thermopower using an MCBJ technique, Tsutsui et al.[80] integrated a nanofabricated microheater into one of the metal wire electrodes and successfully created temperature differential across the junction. The thermovoltage measurement was subsequently performed in a fashion similar to those performed by Reddy et al.

Using the techniques described above, a variety of interesting thermoelectric properties have been experimentally observed in different MJs, including length dependence, temperature dependence, molecule–electrode contact effect, sign-switching of thermopower, quantum interference effect, and gating effect. In the following, we will present recent experimental observations on these topics.

Length Dependence: The dependence of thermopower on molecular length has been experimentally investigated in various molecular systems. It has been found that the variation in magnitude and sign of the Seebeck coefficient with increase of molecular length is closely related to the structure of molecular core and molecule–electrode contact. For example, Malen et al.[79] showed that the Seebeck coefficient increases linearly with molecular length in aromatic MJs, such as Au–phenylenediames–Au and Au–phenylenedithiols–Au junctions, while it decreases linearly in saturated MJs, such as Au–alkanedithiols–Au junctions (**Figure 19**a). This observation agrees well with the results of the first measurement by Reddy et al. However, Widawsky et al.[77] observed a nonlinear increase in Seebeck coefficient with length for aromatic oligophenyls molecules connected to Au electrodes through Au—C bond (Figure 19b). Further, they also showed that the Seebeck coefficient of alkane MJs with Au—C bond is nearly independent of molecular length.
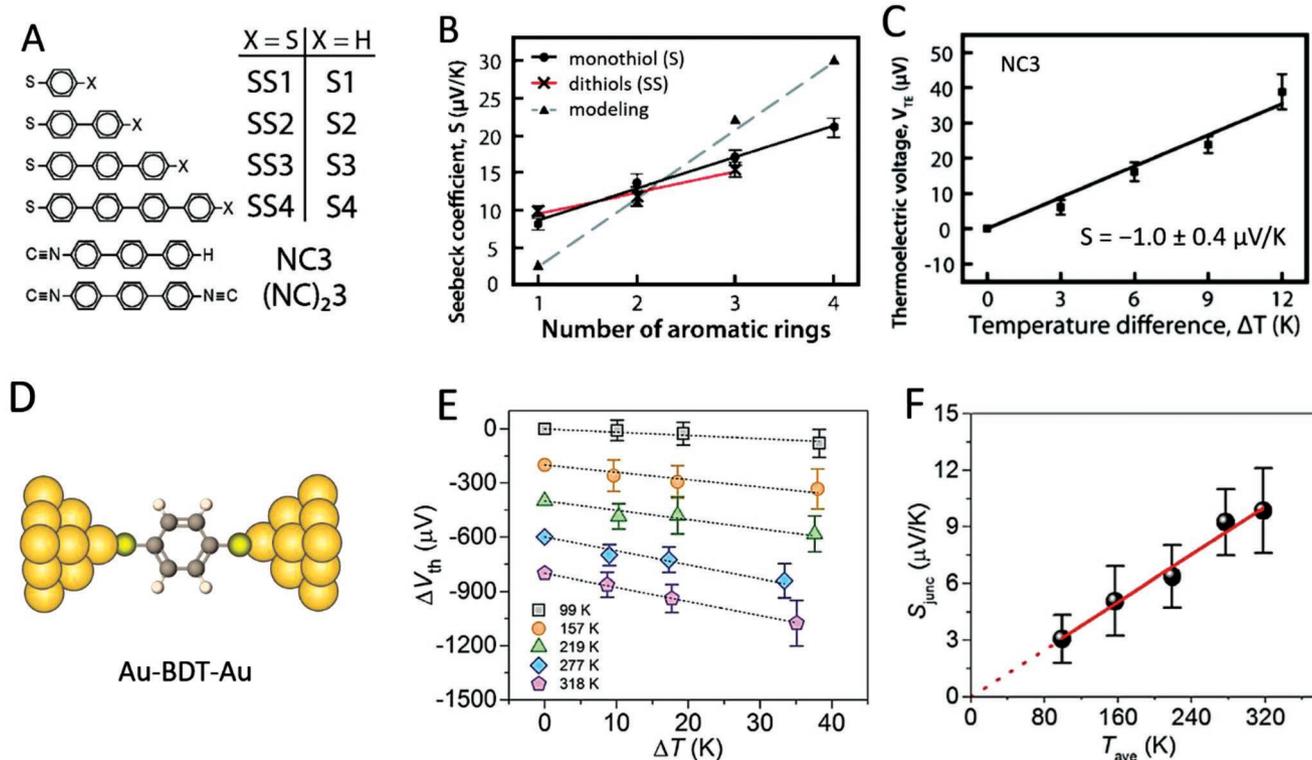
**ADVANCED
SCIENCE NEWS**

www.advancedsciencenews.com

**ADVANCED
FUNCTIONAL
MATERIALS**

www.afm-journal.de

Figure 20. Experimental measurements of thermopower as a function of contact chemistry and average ambient temperature. A) Structure of mono-thiol-, dithiol-, and isocyanide-terminated aromatic molecules. B) Measured thermopower of dithiol and monothiol junctions along with computed values for dithiol junctions. C) Measure thermovoltage as a function of temperature difference for Au–NC3–Au junctions. A–C) Reproduced with permission.[81b] Copyright 2011, American Chemical Society. D) Schematic of a Au–benzenedithiol (BDT)–Au junction. E) Measured thermovoltage as a function of temperature difference at different average ambient temperature. F) Measured thermopower as a function of average ambient temperature for BDT molecule. D–F) Reproduced with permission.[88] Copyright 2016, American Physical Society.

Recently, Dell et al.[85] reported that the Seebeck coefficient of molecules can also switch its sign when molecular length increases, indicating an alteration of dominant charge carriers. Specifically, as shown in Figure 19c, the measured Seebeck coefficient of a family of thiophene-1,1-dioxide $(TDO)_n$ molecules changes its sign from positive to negative as the number of TDO units is increased. The transition occurs at TDO_3. This clearly indicates that the dominant charge carriers change from holes to electrons with the increase of molecular length.

The length dependence of thermopower in DNA-based MJs has also been studied. In a recent work, Li et al.[78] reported that despite the linear decrease in conductance with length, the Seebeck coefficient of 5'-A(CG)$_n$T-3' DNA molecules is small (<2 uV K^{-1}) and insensitive to molecular length. This is attributed to the dominant hopping transport in GC rich DNA sequences. In contrast, for adenine-thymine (AT) rich DNA sequences (ACGC(AT)$_m$GCGT and 5'-ACGC(AT)$_{m-1}$AGCGT-3'), they found that when the inserted AT block is shorter than four base pairs, it serves as a tunneling barrier with conductance decreases exponentially and Seebeck coefficient increases linearly with the block length. However, when the inserted AT block is longer than four base pairs, the charge transport mechanism switches from tunneling to hopping, leading to a conductance that is weakly length-dependent and a small Seebeck coefficient that is insensitive to molecular length. These observations suggest that the thermopower of

DNA molecules is not only dependent on molecular length, it is also closely associated with the sequence and the transport regime.

Molecule–Electrode Contact Effect: The molecule–electrode contact interface has been reported to play a significant role in determining charge transport in MJs.[86] Similarly, recent thermopower measurements reveal that the contact effect also has a crucial impact on thermoelectric properties of MJs. For example, experimental studies have shown that oligophenylene MJs with Au–thiol (SH) and Au–carbon (C) contact have positive Seebeck coefficient, whereas the same MJs with Au-isocyanide (NC) contact show a negative and much smaller Seebeck coefficient (**Figure 20**a–c).[77,79] In addition, despite the same sign, the oligophenylene MJs with Au–C contact usually reveal higher Seebeck coefficient values than those with Au–S contact, especially when molecular length is increased. This enhancement in Au–C linked MJs is attributed to a gateway state induced by the Au−C bond that modifies the transmission function profile of the MJs.[77] Further theoretical investigation suggests that, when coupled to Au electrodes, isocynide (NC), nitrile (CN), and amine (NH$_2$) anchored junctions, with electron transfer out of the molecule, exhibit a strong downshift in the energies of frontier molecular orbitals, whereas −SH and −OH anchored molecular junctions, with charge transfer into the molecule, exhibit a smaller downshift. These studies suggest that the sign of the thermopower of molecular junctions is
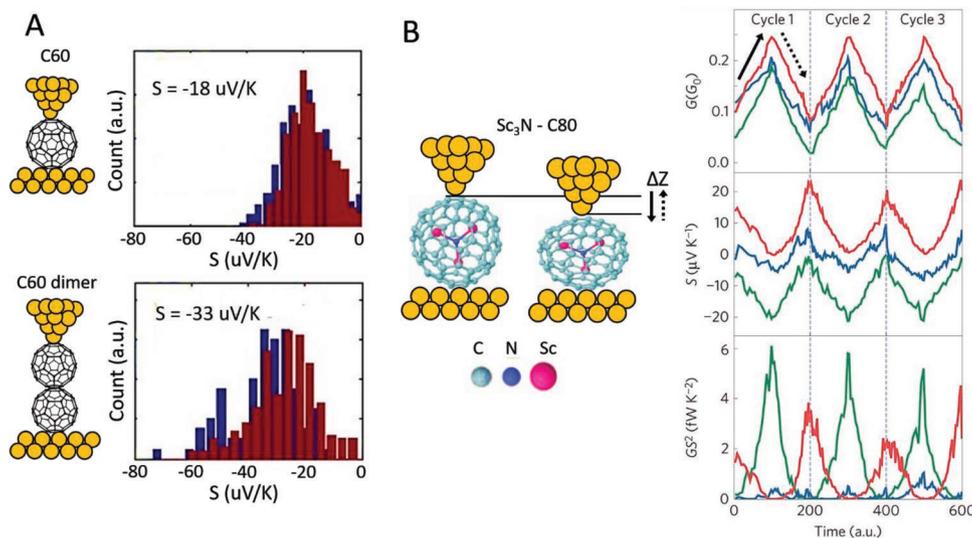
Figure 21. Thermopower measurements of fullerene C60 and its derivatives. A) Measured thermopower for C60 monomer junctions (upper panel) and stacked C60 dimer junctions, schematically shown in the left panel. The thermopower of stacked C60 dimer junctions doubles that of the C60 dimer junctions. Reproduced with permission.[89] Copyright 2013, American Chemical Society. B) The response of electrical conductance G, thermopower S, and power factor GS^2 of Au–Sc$_3$N@C80–Au junctions to external pressure (mechanical compression and extension). The magnitude and sign of the thermopower depend strongly on the orientation and applied pressure. Reproduced with permission.[91] Copyright 2015, Springer Nature.

closely related to the HOMO–LUMO energies and electronegativity of isolated molecules.[87]

Temperature Dependence: Kim et al.[88] recently investigated the influence of average ambient temperature on the thermopower of MJs. Using temperature variable STM-BJ technique, they measured the Seebeck coefficient and electrical conductance of Au–benzenedithiol–Au junctions over a range of temperatures (100–300 K). Their results reveal that the Seebeck coefficient increases linearly with temperature (Figure 20d–f), while the electrical conductance is independent of temperature. This work confirms the predictions of the Landauer theory that the thermoelectric properties of MJs depend linearly on ambient temperature.

Fullerene Derivative Junctions: Fullerene (C60) and its derivatives have been considered as promising candidates for molecular-scale electronic and thermoelectric applications due to their efficient charge transport and interesting thermoelectric transport properties. The thermoelectric properties of C60 MJ was recently explored by Evangeli et al.[89] In their measurements, STM imaging was employed to locate C60 molecules on a Au (111) surface prior to thermopower measurement. By doing so, they were able to construct C60 dimers via trapping one C60 on the tip and subsequently stacking it onto a C60 on the substrate surface. The thermopower measurements reveal that the Seebeck coefficient of C60 dimers is −33 μV K^{-1}, which is almost double that of a single C60 base junction, which has a Seebeck coefficient of −18 μV K^{-1} (**Figure 21**a). The thermopower enhancement in the dimer configuration is attributed to intermolecular interaction between the two C60 molecules.

In addition, Lee et al.[90] studied the thermoelectric properties of three fullerene derivatives (C82, Gd@C82, and Ce@C82). They found that the Seebeck coefficient for all three fullerene derivatives is negative (electron-conduction). The Gd@C82 and Ce@C82 junctions yield a large Seebeck coefficient of −31.6 and −30.0 μV K^{-1}, respectively. However, a smaller Seebeck

coefficient of −22.7 μV K^{-1} is observed for C82 junctions. Their electrical conductance, on the other hand, remains comparable for all three junctions. Their work hints that, although not contributing to transport, the encapsulated metal atom inside the fullerene cage could substantially change the electronic and geometrical structure of molecule. More recently, Rincon-Garcia et al.[91] experimentally investigated the influence of applied pressure on the thermopower of the endohedral fullerene Sc3N@C80 between gold electrodes. Using an STM based technique, they applied pressure to an isolated Sc3N@ C80 molecule by compressing the molecule with an STM tip. Upon compression, the electrical conductance of Sc3N@C80 increases, whereas the Seebeck coefficient switches from positive side toward negative side with both its sign and magnitude changed. This process is reversible and the detailed Seebeck coefficient values vary from molecule to molecule. The group was further able to show that this phenomenon is not present in C60 MJ. Therefore, this work successfully demonstrated the bithermoelectricity effect in Sc3N@C80 MJ system, in which the sign and magnitude of the thermopower of a given material can be tuned by external stimuli. The physical mechanism of the observed bithermoelectricity is attributed to the fact that the transmission resonance of the junction is very close to the Fermi energy and it can be tuned to cross the Fermi energy via external pressure or varying the molecular orientation.

QI Effect: QI effect in MJs is proposed as an avenue for highly efficient thermoelectric energy conversion at room temperature.[19b] Toward this goal, Miao et al.[92] recently studied the influence of QI on the thermopower of OPE molecules (**Figure 22**a,b). Specifically, they show that the Seebeck coefficient of meta-OPE junction is ≈20 μV K^{-1}, doubling that of a para-OPE junction, ≈10 μV K^{-1}. This enhancement is mainly because the meta configuration of the central ring of the OPE molecule induces destructive π-interference which leads to a steeper slope of the transmission function at the Fermi energy.
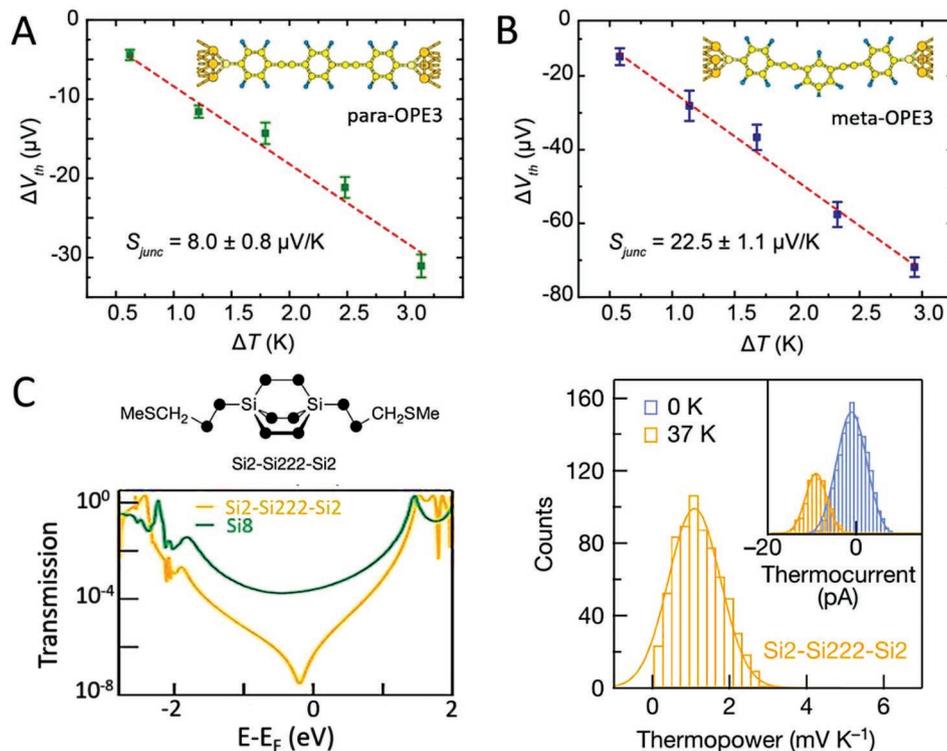
**ADVANCED
SCIENCE NEWS**
www.advancedsciencenews.com

**ADVANCED
FUNCTIONAL
MATERIALS**
www.afm-journal.de

Figure 22. Experimental investigations on the influence of quantum interference (QI) on thermopower of molecular junctions. A) Measured thermopower of Au–para OPE–Au junction. B) Measured thermopower of Au–meta OPE–Au junction. A,B) Reproduced with permission.[92] Copyright 2018, American Chemical Society. C) Left panel: Structure and transmission function of a saturated silicon-based molecule with a functionalized bicyclo[2.2.2] octasilane moiety (Si2-Si222-Si2). A clear dip near the Fermi energy is observed due to destructive QI effect in Si2-Si222-Si2 junction. Right panel: Measured thermopower of the Si2-Si222-Si2 junctions. Inset: Thermocurrent of the junction. Reproduced with permission.[93] Copyright 2018, Springer Nature.

Similarly, a recent study by Garner et al.[93] reports that this concept can also be applied to destructive σ-interference in a σ-orbital system (Figure 22c). Specifically, they demonstrate that a saturated silicon-based molecule with a functionalized bicyclo[2.2.2]octasilane moiety (Si2-Si222-Si2) can exhibit strong destructive QI in its σ-system. Such destructive QI leads to an extreme suppression of the electrical conductance of the junction and a giant Seebeck coefficient of ≈1 mV K^{-1}. However, despite the contribution to the enhancement in thermopower, an obvious drawback of the destructive QI effect is that the electrical conductance of the MJ is greatly reduced, which eventually leads to a low power factor ($G_e S^2$). Recent studies have suggested that constructive QI effects that help improving both electrical conductance and thermopower should offer unique opportunity to achieving high-efficiency thermoelectric energy conversion in MJs.[11c] Future investigations along this line are therefore needed and expected.

Electrostatic Gating: Key to optimizing the thermoelectric performance of MJs is the ability to manipulate their charge transmission profile near the Fermi energy (E_F), as their thermoelectric properties are determined by the magnitude and the derivative of the transmission at E_F. It has been shown that tuning of the position of frontier molecular orbitals relative to E_F can be achieved in a three-terminal configuration constructed with EMBJ based technique.[6a,c] To create a three-terminal device using the EMBJ setup, a gold wire was first fabricated with e-beam lithography on a doped Si layer coated

with thin dielectric material. Then, a nanogap can be created by passing large current through the wire to cause migration of metal atoms and eventually break the wire. The two sides of the broken wire serve as the source and drain electrodes with the Si back gate acting as the gate electrode. However, past efforts in thermoelectric measurement using such method were limited due to difficulties in establishing temperature gradient across the nanogap. Recently, Kim et al.[6b] showed that an extremely large temperature difference can be achieved in the nanogap by introducing a microheater to one side of the nanogap. Using their three-terminal platform, they successfully demonstrate that the thermopower of MJs can be greatly enhanced via electrostatic gating (**Figure 23**). Specifically, in their measurements, the magnitudes of Seebeck coefficients of both Au–BDT–Au junction and Au–C60–Au junction show a strong dependence on the gate voltage. For C60 junctions, the largest Seebeck coefficient of ≈60 µV K^{-1} is achieved at a gate voltage of −2 V. The gating effect is well correlated with the shift of the transmission characteristics with respect to E_F under a certain gate voltage. Therefore, this work proves the feasibility of using electrostatic gating to tune thermoelectric properties of MJs.

5. Conclusions and Perspectives

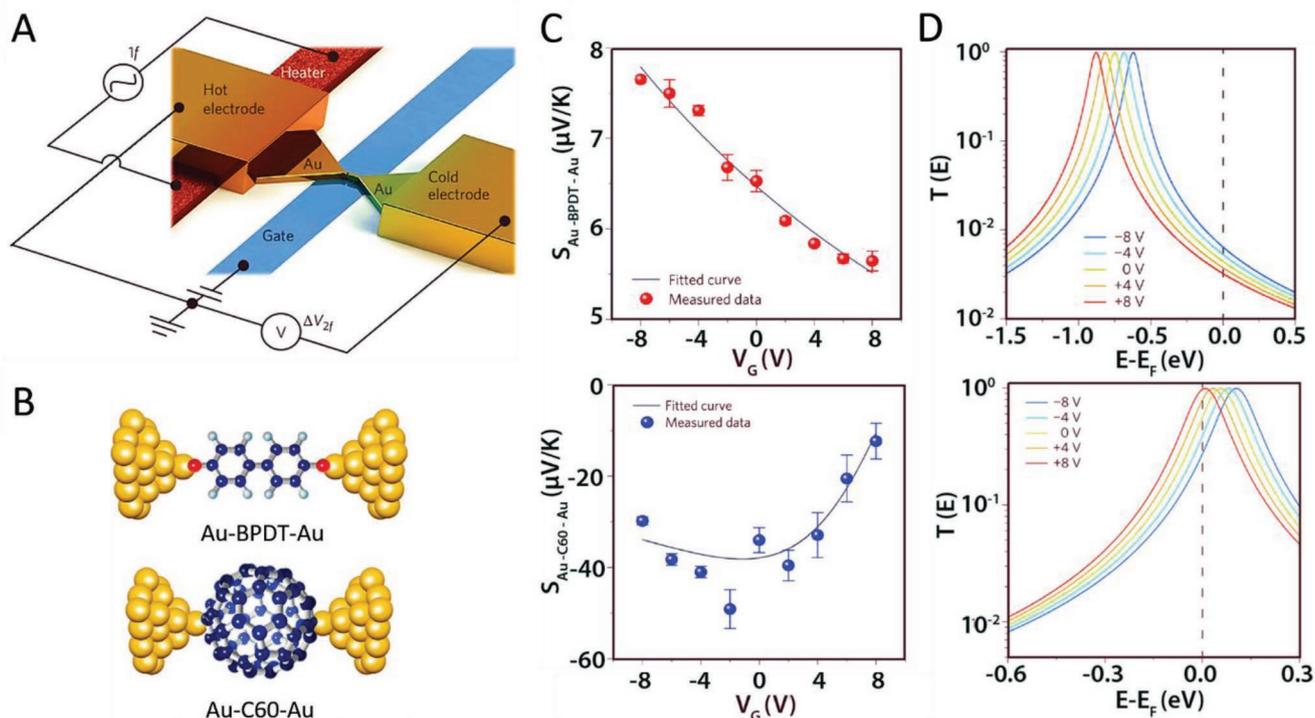The past two decades have witnessed remarkable advances in understanding how energy is transported, dissipated, and

**ADVANCED
SCIENCE NEWS**
www.advancedsciencenews.com

**ADVANCED
FUNCTIONAL
MATERIALS**
www.afm-journal.de

Figure 23. Tuning thermopower of molecular junctions via electrostatic gating. A) Schematic of the electromigrated break junction (EMBJ) setup with integrated heater (red) and gate electrode (blue). B) Molecular junctions studied. C) Measured Seebeck coefficient as a function of gate voltage V_G for Au–biphenyldithol(BPDT)–Au (upper) and Au–C60–Au (lower) junctions. D) Calculated transmission function of the junction under different gate voltages. The gate voltage shifts the position of the transmission peak relative to the Fermi energy, leading to changes in the Seebeck coefficient of the junction. Reproduced with permission.[6b] Copyright 2014, Springer Nature.

converted in MJ devices. In this review, we have systematically discussed recent progresses made in probing thermal and thermoelectric properties of MJs from both experimental and theoretical perspectives. Research into thermal and thermoelectric properties together with the charge transport studies have offered much deeper insights into the fundamental correlation between the electronic structure of MJs and their functionality and performance. More importantly, promising transport characteristics, such as high thermal conductivity, large thermopower, and figure of merit ZT, have been theoretically predicted or experimentally observed in carefully designed MJs. Concepts and ideas borrowed from charge transport studies, such as quantum interference effect, also continue to inspire new design strategies to tailor the thermal and thermoelectric transport in MJs. Further, thermoelectric functions beyond those achievable with conventional semiconductor materials, such as bithermoelectricity, have also been demonstrated in specific MJs. We expect that this newly gained knowledge and observed phenomena will inspire new research that may eventually lead to novel applications in electronics and energy conversion.

Despite the great potential of MJ devices in a wide range of thermal applications, studying thermal and thermoelectric properties of MJs in a more reliable and controlled manner poses significant challenges for both experimentalists and theoreticians. From the experimental point of view, there are a few outstanding hurdles in the field that need to be overcome. First, the thermal conductance of single molecule junctions was

inaccessible due to difficulties in sensing small temperature changes induced by heat flow through a single molecule. This challenge has very recently been overcome[52] by employing custom-fabricated scanning thermal probes.[43] We expect that these advances will open the door for testing heat transfer laws at molecular scale and systematically exploring theoretical proposals in optimizing thermal transport in MJs, especially strategies to suppress phononic contributions.

The key challenge in thermoelectric applications of MJs is to demonstrate high efficiency (i.e., high power factor $G_e S^2$ and figure of merit ZT). This requires appropriate designs to enhance both electrical conductance and thermopower of an MJ while suppressing its thermal conductance. However, from past experimental measurements, the electrical conductance and thermopower of an MJ are often negatively correlated, meaning enhancements in thermopower are accompanied by decreases in electrical conductance. Although the ideal approach to the molecular design of MJs remain elusive at this point, introducing constructive quantum interference has been proposed as one of the possible mechanisms to significantly enhance electrical conductance and thermopower at the same time. In addition, the development of three-terminal MJ devices also deserves more attention as it has been proven to effectively tune the location of transmission of an MJ.

Experimentally probing local heat dissipation and temperature change in the molecular region is also of paramount importance for both validating existing theoretical models and

**ADVANCED
SCIENCE NEWS**
www.advancedsciencenews.com

**ADVANCED
FUNCTIONAL
MATERIALS**
www.afm-journal.de

offering insights into the operation limits of MJ devices. Given the tiny size of the molecular region and flexible molecular orientation, current experimental techniques are not capable of directly measuring local temperature of the molecular region and experimental results based on indirect measurements often show large variations. Therefore, experimental techniques that have both high thermal and spatial resolution are required.

From a theoretical standpoint, the development of accurate computational tools is urgent. Existing calculation methods have difficulties in precisely determining the location and magnitude of transmission characteristics with respect to Fermi energy. This makes it challenging to provide a quantitative explanation for experimental observations and often leads to overestimation or underestimation of the device performance.

Finally, we note that key to progress in the multidisciplinary area is harnessing expertise from chemistry, engineering, and physics, to both establish the mechanisms of transport in single molecule junctions and to employ insights from single molecule studies to develop materials and devices based on molecular junctions for energy conversion and electronics. Given recent advances there is no doubt that the field will continue to progress and achieve important scientific and economic impacts.

Conflict of Interest

The authors declare no conflict of interest.

[1] a) D. Xiang, X. Wang, C. Jia, T. Lee, X. Guo, *Chem. Rev.* **2016**, *116*, 4318; b) N. J. Tao, *Nat. Nanotechnol.* **2006**, *1*, 173; c) S. V. Aradhya, L. Venkataraman, *Nat. Nanotechnol.* **2013**, *8*, 399; d) R. M. Metzger, *Chem. Rev.* **2015**, *115*, 5056; e) M. L. Perrin, E. Burzuri, H. S. J. van der Zant, *Chem. Soc. Rev.* **2015**, *44*, 902.

[2] K. Wang, B. Xu, *Top. Curr. Chem.* **2017**, *375*, 17.

[3] C. Huang, A. V. Rudnev, W. Hong, T. Wandlowski, *Chem. Soc. Rev.* **2015**, *44*, 889.

[4] a) C. Jia, A. Migliore, N. Xin, S. Huang, J. Wang, Q. Yang, S. Wang, H. Chen, D. Wang, B. Feng, Z. Liu, G. Zhang, D.-H. Qu, H. Tian, M. A. Ratner, H. Q. Xu, A. Nitzan, X. Guo, *Science* **2016**, *352*, 1443; b) T. A. Su, H. Li, M. L. Steigerwald, L. Venkataraman, C. Nuckolls, *Nat. Chem.* **2015**, *7*, 215; c) A. K. Ismael, K. Wang, A. Vezzoli, M. K. Al-Khaykanee, H. E. Gallagher, I. M. Grace, C. J. Lambert, B. Xu, R. J. Nichols, S. J. Higgins, *Angew. Chem., Int. Ed.* **2017**, *56*, 15378.

[5] a) B. Capozzi, J. Xia, O. Adak, E. J. Dell, Z.-F. Liu, J. C. Taylor, J. B. Neaton, L. M. Campos, L. Venkataraman, *Nat. Nanotechnol.* **2015**, *10*, 522; b) C. Guo, K. Wang, E. Zerah-Harush, J. Hamill, B. Wang, Y. Dubi, B. Xu, *Nat. Chem.* **2016**, *8*, 484; c) X. Chen, M. Roemer, L. Yuan, W. Du, D. Thompson, E. del Barco, C. A. Nijhuis, *Nat. Nanotechnol.* **2017**, *12*, 797.

[6] a) D. Xiang, H. Jeong, D. Kim, T. Lee, Y. Cheng, Q. Wang, D. Mayer, *Nano Lett.* **2013**, *13*, 2809; b) Y. Kim, W. Jeong, K. Kim, W. Lee, P. Reddy, *Nat. Nanotechnol.* **2014**, *9*, 881; c) H. Song, Y. Kim, Y. H. Jang, H. Jeong, M. A. Reed, T. Lee, *Nature* **2009**, *462*, 1039.

[7] a) M. L. Perrin, R. Frisenda, M. Koole, J. S. Seldenthuis, A. C. GilJose, H. Valkenier, J. C. Hummelen, N. Renaud, F. C. Grozema, J. M. Thijssen, D. Dulić, S. J. van der ZantHerre, *Nat. Nanotechnol.* **2014**, *9*, 830; b) X. Bingqian, D. Yonatan, *J. Phys.: Condens. Matter* **2015**, *27*, 263202; c) R. Pati, M. McClain, A. Bandyopadhyay, *Phys. Rev. Lett.* **2008**, *100*, 246801.

[8] a) J. Zhou, K. Wang, B. Xu, Y. Dubi, *J. Am. Chem. Soc.* **2018**, *140*, 70; b) E. D. Fung, O. Adak, G. Lovat, D. Scarabelli, L. Venkataraman, *Nano Lett.* **2017**, *17*, 1255.

[9] a) P. C. Mondal, C. Fontanesi, D. H. Waldeck, R. Naaman, *Acc. Chem. Res.* **2016**, *49*, 2560; b) Z. Xie, T. Z. Markus, S. R. Cohen, Z. Vager, R. Gutierrez, R. Naaman, *Nano Lett.* **2011**, *11*, 4652; c) A. C. Aragonès, D. Aravena, J. I. Cerdá, Z. Acís-Castillo, H. Li, J. A. Real, F. Sanz, J. Hihath, E. Ruiz, I. Díez-Pérez, *Nano Lett.* **2016**, *16*, 218.

[10] C. Bruot, J. L. Palma, L. Xiang, V. Mujica, M. A. Ratner, N. Tao, *Nat. Commun.* **2015**, *6*, 8032.

[11] a) X. Liu, S. Sangtarash, D. Reber, D. Zhang, H. Sadeghi, J. Shi, Z.-Y. Xiao, W. Hong, C. J. Lambert, S.-X. Liu, *Angew. Chem., Int. Ed.* **2017**, *56*, 173; b) C. Jia, M. Famili, M. Carlotti, Y. Liu, P. Wang, I. M. Grace, Z. Feng, Y. Wang, Z. Zhao, M. Ding, X. Xu, C. Wang, S.-J. Lee, Y. Huang, R. C. Chiechi, C. J. Lambert, X. Duan, *Sci. Adv.* **2018**, *4*, eaat8237; c) K. Wang, A. Vezzoli, I. M. Grace, M. McLaughlin, R. J. Nichols, B. Xu, C. J. Lambert, S. J. Higgins, *Chem. Sci.* **2019**, *10*, 2396; d) Y. Geng, S. Sangtarash, C. Huang, H. Sadeghi, Y. Fu, W. Hong, T. Wandlowski, S. Decurtins, C. J. Lambert, S.-X. Liu, *J. Am. Chem. Soc.* **2015**, *137*, 4469.

[12] M. Paulsson, S. Datta, *Phys. Rev. B* **2003**, *67*, 241403.

[13] a) L. Cui, R. Miao, C. Jiang, E. Meyhofer, P. Reddy, *J. Chem. Phys.* **2017**, *146*, 092201; b) Y. Dubi, M. Di Ventra, *Rev. Mod. Phys.* **2011**, *83*, 131; c) L. Rincón-García, C. Evangeli, G. Rubio-Bollinger, N. Agraït, *Chem. Soc. Rev.* **2016**, *45*, 4285.

[14] a) J. P. Bergfield, M. A. Solis, C. A. Stafford, *ACS Nano* **2010**, *4*, 5314; b) C. M. Finch, V. M. García-Suárez, C. J. Lambert, *Phys. Rev. B* **2009**, *79*, 033405; c) M. Famili, I. M. Grace, Q. Al-Galiby, H. Sadeghi, C. J. Lambert, *Adv. Funct. Mater.* **2018**, *28*, 1703135; d) A. Henry, G. Chen, *Phys. Rev. Lett.* **2008**, *101*, 235502.

[15] a) A. Shakouri, *Proc. IEEE* **2006**, *94*, 1613; b) L. Cui, R. Miao, K. Wang, D. Thompson, L. A. Zotti, J. C. Cuevas, E. Meyhofer, P. Reddy, *Nat. Nanotechnol.* **2018**, *13*, 122.

[16] a) B. Li, L. Wang, G. Casati, *Phys. Rev. Lett.* **2004**, *93*, 184301; b) D. Segal, A. Nitzan, *Phys. Rev. Lett.* **2005**, *94*, 034301; c) F. Giazotto, T. T. Heikkilä, A. Luukanen, A. M. Savin, J. P. Pekola, *Rev. Mod. Phys.* **2006**, *78*, 217; d) O.-P. Saira, M. Meschke, F. Giazotto, A. M. Savin, M. Möttönen, J. P. Pekola, *Phys. Rev. Lett.* **2007**, *99*, 027203.

[17] a) L. Wang, B. Li, *Phys. Rev. Lett.* **2007**, *99*, 177208; b) L. Wang, B. Li, *Phys. Rev. Lett.* **2008**, *101*, 267203.

[18] a) R. Landauer, *IBM J. Res. Dev.* **1957**, *1*, 223; b) J. Landauer, *J. Phys.: Condens. Matter* **1989**, *1*, 8099; c) M. Büttiker, Y. Imry, R. Landauer, S. Pinhas, *Phys. Rev. B* **1985**, *31*, 6207.

[19] a) S. Datta, *Quantum Transport: Atom to Transistor*, Cambridge University Press, New York **2005**; b) C. J. Lambert, *Chem. Soc. Rev.* **2015**, *44*, 875.

[20] J. C. Klöckner, M. Matt, P. Nielaba, F. Pauly, J. C. Cuevas, *Phys. Rev. B* **2017**, *96*, 205405.

**ADVANCED
SCIENCE NEWS**

www.advancedsciencenews.com

**ADVANCED
FUNCTIONAL
MATERIALS**

www.afm-journal.de

[21] K. Esfarjani, M. Zebarjadi, Y. Kawazoe, *Phys. Rev. B* **2006**, *73*, 085406.

[22] J. C. Klöckner, R. Siebler, J. C. Cuevas, F. Pauly, *Phys. Rev. B* **2017**, *95*, 245404.

[23] P. N. Butcher, *J. Phys.: Condens. Matter* **1990**, *2*, 4869.

[24] W. Lee, K. Kim, W. Jeong, L. A. Zotti, F. Pauly, J. C. Cuevas, P. Reddy, *Nature* **2013**, *498*, 209.

[25] a) U. Sivan, Y. Imry, *Phys. Rev. B* **1986**, *33*, 551; b) R. Lake, S. Datta, *Phys. Rev. B* **1992**, *46*, 4757.

[26] a) S. Lepri, R. Livi, A. Politi, *Phys. Rep.* **2003**, *377*, 1; b) A. Dhar, *Adv. Phys.* **2008**, *57*, 457.

[27] D. Segal, A. Nitzan, P. Hänggi, *J. Chem. Phys.* **2003**, *119*, 6840.

[28] H. Sadeghi, S. Sangtarash, C. J. Lambert, *Nano Lett.* **2015**, *15*, 7467.

[29] J. C. Klöckner, M. Bürkle, J. C. Cuevas, F. Pauly, *Phys. Rev. B* **2016**, *94*, 205425.

[30] T. Markussen, *J. Chem. Phys.* **2013**, *139*, 244101.

[31] a) D. Z. Manrique, C. Huang, M. Baghernejad, X. Zhao, O. A. Al-Owaedi, H. Sadeghi, V. Kaliginedi, W. Hong, M. Gulcur, T. Wandlowski, M. R. Bryce, C. J. Lambert, *Nat. Commun.* **2015**, *6*, 6389; b) Y. Li, M. Buerkle, G. Li, A. Rostamian, H. Wang, Z. Wang, D. R. Bowler, T. Miyazaki, L. Xiang, Y. Asai, G. Zhou, N. Tao, *Nat. Mater.* **2019**, *18*, 357.

[32] J. C. Klöckner, J. C. Cuevas, F. Pauly, *Phys. Rev. B* **2017**, *96*, 245419.

[33] a) T. Luo, J. R. Lloyd, *J. Heat Transfer* **2009**, *132*, 032401; b) Z. Wang, J. A. Carter, A. Lagutchev, Y. K. Koh, N.-H. Seong, D. G. Cahill, D. D. Dlott, *Science* **2007**, *317*, 787; c) J. C. Duda, C. B. Saltonstall, P. M. Norris, P. E. Hopkins, *J. Chem. Phys.* **2011**, *134*, 094704.

[34] L. Hu, L. Zhang, M. Hu, J.-S. Wang, B. Li, P. Keblinski, *Phys. Rev. B* **2010**, *81*, 235427.

[35] J. V. Goicochea, M. Hu, B. Michel, D. Poulikakos, *J. Heat Transfer* **2011**, *133*, 082401.

[36] D. Huang, R. Ma, T. Zhang, T. Luo, *ACS Appl. Mater. Interfaces* **2018**, *10*, 28159.

[37] M. G. Menezes, A. Saraiva-Souza, J. Del Nero, R. B. Capaz, *Phys. Rev. B* **2010**, *81*, 012302.

[38] Q. Li, I. Duchemin, S. Xiong, G. C. Solomon, D. Donadio, *J. Phys. Chem. C* **2015**, *119*, 24636.

[39] J. Ren, P. Hänggi, B. Li, *Phys. Rev. Lett.* **2010**, *104*, 170601.

[40] F. Zhan, N. Li, S. Kohler, P. Hänggi, *Phys. Rev. E* **2009**, *80*, 061115.

[41] M. Famili, I. Grace, H. Sadeghi, C. J. Lambert, *ChemPhysChem* **2017**, *18*, 1234.

[42] G. Kiršanskas, Q. Li, K. Flensberg, G. C. Solomon, M. Leijnse, *Appl. Phys. Lett.* **2014**, *105*, 233102.

[43] L. Cui, W. Jeong, S. Hur, M. Matt, J. C. Klöckner, F. Pauly, P. Nielaba, J. C. Cuevas, E. Meyhofer, P. Reddy, *Science* **2017**, *355*, 1192.

[44] J. C. Love, L. A. Estroff, J. K. Kriebel, R. G. Nuzzo, G. M. Whitesides, *Chem. Rev.* **2005**, *105*, 1103.

[45] R. Y. Wang, R. A. Segalman, A. Majumdar, *Appl. Phys. Lett.* **2006**, *89*, 173113.

[46] D. G. Cahill, *Rev. Sci. Instrum.* **1990**, *61*, 802.

[47] M. D. Losego, M. E. Grady, N. R. Sottos, D. G. Cahill, P. V. Braun, *Nat. Mater.* **2012**, *11*, 502.

[48] P. J. O'Brien, S. Shenogin, J. Liu, P. K. Chow, D. Laurencin, P. H. Mutin, M. Yamaguchi, P. Keblinski, G. Ramanath, *Nat. Mater.* **2013**, *12*, 118.

[49] S. Majumdar, J. A. Sierra-Suarez, S. N. Schiffres, W.-L. Ong, C. F. Higgs, A. J. H. McGaughey, J. A. Malen, *Nano Lett.* **2015**, *15*, 2985.

[50] T. Meier, F. Menges, P. Nirmalraj, H. Hölscher, H. Riel, B. Gotsmann, *Phys. Rev. Lett.* **2014**, *113*, 060801.

[51] N. Mosso, U. Drechsler, F. Menges, P. Nirmalraj, S. Karg, H. Riel, B. Gotsmann, *Nat. Nanotechnol.* **2017**, *12*, 430.

[52] L. Cui, S. Hur, Z. A. Akbar, J. C. Klöckner, W. Jeong, F. Pauly, S.-Y. Jang, P. Reddy, E. Meyhofer, *Nature* **2019**, *572*, 628.

[53] L. A. Zotti, M. Bürkle, F. Pauly, W. Lee, K. Kim, W. Jeong, Y. Asai, P. Reddy, J. C. Cuevas, *New J. Phys.* **2014**, *16*, 015004.

[54] D. Segal, A. Nitzan, *J. Chem. Phys.* **2002**, *117*, 3915.

[55] M. Galperin, A. Nitzan, M. A. Ratner, *Phys. Rev. B* **2007**, *75*, 155312.

[56] Y.-C. Chen, M. Zwolak, M. Di Ventra, *Nano Lett.* **2005**, *5*, 621.

[57] R. D'Agosta, N. Sai, M. Di Ventra, *Nano Lett.* **2006**, *6*, 2935.

[58] a) M. Galperin, K. Saito, A. V. Balatsky, A. Nitzan, *Phys. Rev. B* **2009**, *80*, 115427; b) R. Härtle, M. Thoss, *Phys. Rev. B* **2011**, *83*, 115414; c) L. Simine, D. Segal, *Phys. Chem. Chem. Phys.* **2012**, *14*, 13820; d) J. Lykkebo, G. Romano, A. Gagliardi, A. Pecchia, G. C. Solomon, *J. Chem. Phys.* **2016**, *144*, 114310; e) G. Romano, A. Gagliardi, A. Pecchia, A. Di Carlo, *Phys. Rev. B* **2010**, *81*, 115438.

[59] a) Z. Huang, B. Xu, Y. Chen, M. Di Ventra, N. Tao, *Nano Lett.* **2006**, *6*, 1240; b) M. Tsutsui, M. Taniguchi, T. Kawai, *Nano Lett.* **2008**, *8*, 3293; c) Z. Huang, F. Chen, R. D'Agosta, P. A. Bennett, M. Di Ventra, N. Tao, *Nat. Nanotechnol.* **2007**, *2*, 698.

[60] Z. Ioffe, T. Shamai, A. Ophir, G. Noy, I. Yutsis, K. Kfir, O. Cheshnovsky, Y. Selzer, *Nat. Nanotechnol.* **2008**, *3*, 727.

[61] D. R. Ward, D. A. Corley, J. M. Tour, D. Natelson, *Nat. Nanotechnol.* **2011**, *6*, 33.

[62] a) S. Sadat, E. Meyhofer, P. Reddy, *Appl. Phys. Lett.* **2013**, *102*, 163110; b) S. Sadat, Y. J. Chua, W. Lee, Y. Ganjeh, K. Kurabayashi, E. Meyhofer, P. Reddy, *Appl. Phys. Lett.* **2011**, *99*, 043106.

[63] D. Segal, *Phys. Rev. B* **2005**, *72*, 165426.

[64] F. Hüser, G. C. Solomon, *J. Phys. Chem. C* **2015**, *119*, 14056.

[65] J. Vacek, J. V. Chocholoušová, I. G. Stará, I. Starý, Y. Dubi, *Nanoscale* **2015**, *7*, 8793.

[66] D. Z. Manrique, Q. Al-Galiby, W. Hong, C. J. Lambert, *Nano Lett.* **2016**, *16*, 1308.

[67] T. Stuyver, P. Geerlings, F. De Proft, M. Alonso, *J. Phys. Chem. C* **2018**, *122*, 24436.

[68] S. Sangtarash, H. Sadeghi, C. J. Lambert, *Phys. Chem. Chem. Phys.* **2018**, *20*, 9630.

[69] M. Strange, J. S. Seldenthuis, C. J. O. Verzijl, J. M. Thijssen, G. C. Solomon, *J. Chem. Phys.* **2015**, *142*, 084703.

[70] O. Karlström, H. Linke, G. Karlström, A. Wacker, *Phys. Rev. B* **2011**, *84*, 113415.

[71] M. Noori, H. Sadeghi, Q. Al-Galiby, S. W. D. Bailey, C. J. Lambert, *Phys. Chem. Chem. Phys.* **2017**, *19*, 17356.

[72] Q. H. Al-Galiby, H. Sadeghi, L. A. Algharagholy, I. Grace, C. Lambert, *Nanoscale* **2016**, *8*, 2428.

[73] C. Jin, G. C. Solomon, *J. Phys. Chem. C* **2018**, *122*, 14233.

[74] R.-Q. Wang, L. Sheng, R. Shen, B. Wang, D. Y. Xing, *Phys. Rev. Lett.* **2010**, *105*, 057202.

[75] D. Ghosh, P. Parida, S. K. Pati, *Appl. Phys. Lett.* **2015**, *106*, 193105.

[76] P. Reddy, S.-Y. Jang, R. A. Segalman, A. Majumdar, *Science* **2007**, *315*, 1568.

[77] J. R. Widawsky, W. Chen, H. Vázquez, T. Kim, R. Breslow, M. S. Hybertsen, L. Venkataraman, *Nano Lett.* **2013**, *13*, 2889.

[78] Y. Li, L. Xiang, J. L. Palma, Y. Asai, N. Tao, *Nat. Commun.* **2016**, *7*, 11294.

[79] J. A. Malen, P. Doak, K. Baheti, T. D. Tilley, R. A. Segalman, A. Majumdar, *Nano Lett.* **2009**, *9*, 1164.

[80] T. Morikawa, A. Arima, M. Tsutsui, M. Taniguchi, *Nanoscale* **2014**, *6*, 8235.

[81] a) A. Tan, S. Sadat, P. Reddy, *Appl. Phys. Lett.* **2010**, *96*, 013110; b) A. Tan, J. Balachandran, S. Sadat, V. Gavini, B. D. Dunietz, S.-Y. Jang, P. Reddy, *J. Am. Chem. Soc.* **2011**, *133*, 8838; c) W. B. Chang, B. Russ, V. Ho, J. J. Urban, R. A. Segalman, *Phys. Chem. Chem. Phys.* **2015**, *17*, 6207.

[82] A. I. Yanson, G. R. Bollinger, H. E. van den Brom, N. Agraït, J. M. van Ruitenbeek, *Nature* **1998**, *395*, 783.

[83] B. Q. Xu, N. J. Tao, *Science* **2003**, *301*, 1221.

[84] J. R. Widawsky, P. Darancet, J. B. Neaton, L. Venkataraman, *Nano Lett.* **2012**, *12*, 354.

[85] E. J. Dell, B. Capozzi, J. Xia, L. Venkataraman, L. M. Campos, *Nat. Chem.* **2015**, *7*, 209.

[86] a) K. Wang, J. M. Hamill, J. Zhou, C. Guo, B. Xu, *Faraday Discuss.* **2014**, *174*, 91; b) C. Jia, X. Guo, *Chem. Soc. Rev.* **2013**, *42*, 5642.

[87] J. Balachandran, P. Reddy, B. D. Dunietz, V. Gavini, *J. Phys. Chem. Lett.* **2012**, *3*, 1962.

[88] Y. Kim, A. Lenert, E. Meyhofer, P. Reddy, *Appl. Phys. Lett.* **2016**, *109*, 033102.

[89] C. Evangeli, K. Gillemot, E. Leary, M. T. González, G. Rubio-Bollinger, C. J. Lambert, N. Agraït, *Nano Lett.* **2013**, *13*, 2141.

[90] S. K. Lee, M. Buerkle, R. Yamada, Y. Asai, H. Tada, *Nanoscale* **2015**, *7*, 20497.

[91] L. Rincón-García, A. K. Ismael, C. Evangeli, I. Grace, G. Rubio-Bollinger, K. Porfyrakis, N. Agraït, C. J. Lambert, *Nat. Mater.* **2016**, *15*, 289.

[92] R. Miao, H. Xu, M. Skripnik, L. Cui, K. Wang, K. G. L. Pedersen, M. Leijnse, F. Pauly, K. Wärnmark, E. Meyhofer, P. Reddy, H. Linke, *Nano Lett.* **2018**, *18*, 5666.

[93] M. H. Garner, H. Li, Y. Chen, T. A. Su, Z. Shangguan, D. W. Paley, T. Liu, F. Ng, H. Li, S. Xiao, C. Nuckolls, L. Venkataraman, G. C. Solomon, *Nature* **2018**, *558*, 415.